Tunable Reflectarrays and Metasurfaces

by

Peng Zhang

A thesis
presented to the University of Waterloo
in fulfillment of the
thesis requirement for the degree of
Master of Applied Science
in
Electrical and Computer Engineering

Waterloo, Ontario, Canada, 2022

Author's Declaration

I hereby declare that I am the sole author of this thesis. This is a true copy of the thesis, including any required final revisions, as accepted by my examiners.

I understand that my thesis may be made electronically available to the public.

Abstract

Fifth-generation (5G) wireless communication networks have been rapidly expanding in recent years. However, due to the higher frequency bands used in 5G applications compared with previous generations, it is more difficult for electromagnetic waves to transmit through the air or pass through buildings. To avoid the costs of increasing assembled antenna density, one possible solution is beam-steering antennas. Reflectarrays and metasurfaces play an important role in beam-steering applications.

Reflectarrays and metasurfaces basically use the same concepts that originated from other types of directive antennas, such as parabolic reflectors, except that the structure size and periodicity of reflectarrays are around half a wavelength, whereas those of metasurfaces are usually sub-wavelength. Reflectarrays and metasurfaces are normally installed on a flat surface that consists of a large amount of well-organized meta units and an illuminating feed antenna. Their working principle is phase discontinuity across the surface. Numerous applications, including wavefront shaping, beam steering, frequency selecting, power amplifying, power combining, etc., are based on this principle.

The construction of dynamically tunable reflectarrays or metasurfaces is relatively easy and can be accomplished by changing the external conditions or adjusting one or more of the unit cell characteristics. All unit cells can be managed the same way to manipulate plane wave reflections and transmission coefficients. The unit cells can also be tuned separately for wavefront shaping, beam steering, etc. In general, intrinsic losses associated with control components, as well as their tunability range, limit the effectiveness of tunable reflectarrays and metasurfaces.

The objective of the present research is to investigate the performance of several possible tunable reflectarrays and metasurfaces used for beam steering. The use of different types of controlling methodology, including mechanical and electrical tuning, is examined in depth. The simulation results demonstrate the possibility of a tunable reflection with a phase shift range over 180°. As well, an electrically tunable reflectarray is realized using varactor diodes.

Acknowledgements

I would like to thank all people who made this thesis possible.

Firstly, my deepest gratitude goes to my supervisor, Professor Raafat Mansour, who has been immensely supportive during my years at the University of Waterloo. I will never forget his encouragement and guidance as I hurdled the obstacles in my research work. I am also grateful for his efforts and patience for every research discussion throughout the entire program.

As well, I would like to express special thanks to my co-supervisor, Professor Safieddin Safavi-Naeini, who, although no longer with us, continues to inspire me.

I would also like to thank Professor Eihab Abdel-Rahman and Professor George Shaker for being the examiners of my thesis.

It has been a great experience for me to be a member of the Center for Integrated RF Engineering team and I obtained lots of help from my lab colleagues. Many thanks to Dr. Luis Gutierrez for his efforts in maintaining an organized lab and for the equipment training he provided. I also appreciate the advice and support for my research work from Johnny, Frank, Matthew, Farzad, Hassan and Arash.

Lastly, I would like to point out that even though it has been really tough in the past two years because of COVID pandemic, I still feel fortunate to have spent part of my life at the University of Waterloo and to have made such good friends.

Dedication

This thesis is dedicated to my parents and my elder sister.

Your love continues to support me, even across the twelve-thousand kilometer distance that separates us.

Table of Contents

List of Figures

List of Tables

Chapter 1

Introduction

1.1 Motivation

A reflectarray antenna consists of a feed antenna and a flat reflecting surface on which are laid a number of elements, distributed in a certain order. The aperture of each element determines the amplitude and phase shift between the reflection and incident field. Reflectarrays have been rapidly developed as an alternative to these high-gain antennas without the disadvantages of conventional reflector antennas and phased array antennas. The reflectarray antenna was first introduced in 1963 [1], when a feed antenna was used to illuminate a short-ended waveguide array with different lengths. Since that time, reflectarray antennas have developed numerous capabilities and potentials, such as point-to-point communication, beam steering, spatial power combining systems, etc.

Similar to reflectarrays, metamaterial whose units are designed to achieve resonance of every single element possess negative relative permittivity and permeability values. Metasurfaces are viewed as "surface metamaterials" that can change the reflection response based on their polarization. These materials are less bulky and can be easily integrated with tunable elements. Metasurfaces also have many applications, like wavefront shaping, lenses, frequency selective surfaces, beam steering antennas, and so on.

There are three main differences between a metasurface and a reflectarray. Firstly, the spacing between adjacent metasurface units and the unit dimensions are smaller than that in a reflectarray, which is usually half a wavelength. Secondly, a metasurface requires competent engineering to suppress surface waves for good dispersion characteristics. The last difference is that a reflectarray needs proper phase distribution of each element, whereas a metasurface functions in a periodic manner.

This thesis explores several ways to achieve beam steering using reflectarrays or metasurfaces.

1.2 Objectives

The thesis objectives are as follows:

1) To investigate the concepts of reflectarrays and metasurfaces for beam-steering applications.

2) To design and simulate different types of metasurfaces and reflectarrays.

3) To fabricate and measure the performance of a prototype unit.

1.3 Thesis Outline

In Chapter 1, the motivation and objectives of this thesis are provided.

In Chapter 2, an overview of metasurfaces and reflectarrays is introduced. Methods to achieve re-configurable reflectarrays and metasurfaces are compared, and applications based on them are addressed.

In Chapter 3, various methods of beam steering by metasurfaces and reflectarrays are discussed and the phase distribution calculation of the whole device is given. As well, the mechanism to achieve tunability is examined in depth. Further, two types of tunable metasurfaces and tunable reflectarrays are discussed and investigated.

In Chapter 4, the layout of an electrically tunable reflectarray is designed. The simulation results and measurement results for biasing network are depicted. The performance of the reflectarray is also discussed.

In Chapter 5, a summary of the contribution of this thesis is presented, followed by some suggestions for future work.

Chapter 2

Literature Review

2.1 Overview

This chapter introduces a literature review of the related topics of reflectarrays and metasurfaces. To understand them, definitions and characteristics are provided. In addition, applications of reflectarrays and metasurfaces are also discussed.

2.2 Reflectarray

2.2.1 Definitions and characteristics

As introduced in the first chapter, the concept of the reflectarray antenna was first brought by Berry, Malech, and Kennedy in 1963[1]. Short-ended waveguides with different lengths were combined as a whole and excited by a far-field beam from a horn antenna. All signals were reflected from the short-ended waveguide and the reflection phase could be controlled by varying the lengths of each waveguide element. Due to the bulkiness and heavyweight of this device, it got discarded soon.

With the start of PCB technology, a combination of reflectarray and microstrip radiators was first mentioned and investigated by Malagisi[2]. Montgomery first used the infinite array method to analyze reflectarray in the same year that demonstrates an infinite array of microstrip elements can obtain phase and amplitude data by integral equation techniques[3]. In late 1980s and early 1990s, to achieve small-sized and low-weight antennas, reflectarrays using PCB technology were developed again.

A typical reflectarray antenna is a device consisting of planar array elements that are excited by a feed antenna as shown in Figure 2.1.

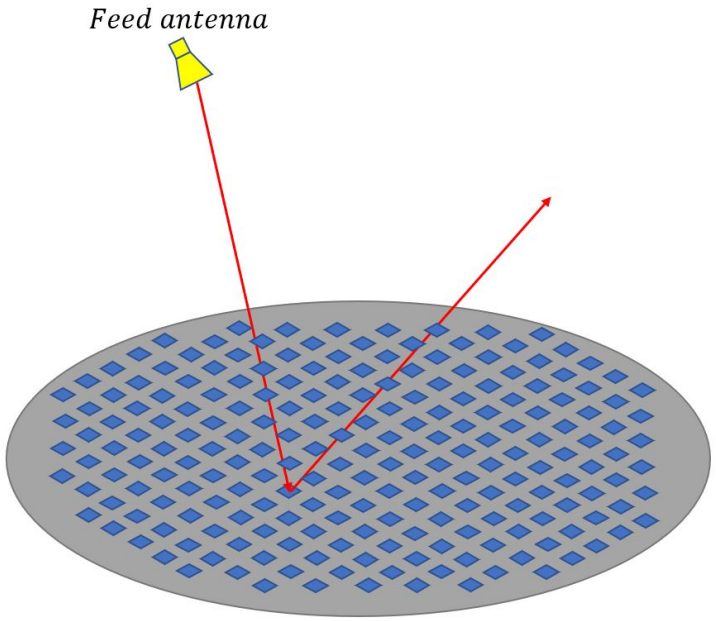

Figure 2.1: Typical geometry of a planar reflectarray antenna

Similar to classic planar antenna arrays[4], a progressive phase distribution assigned to the elements is able to focus the beam in a certain direction. For reflectarray systems, the feed antenna position is also important for performance. Normally, the elements of the reflectarray are considered to be in the feed antenna's far-field thus the incident wave on each element may be viewed as a plane wave exciting the reflectarray at a certain incident angle. The feed antenna generates a spherical wave that originates at the antenna's phase center. The phase of incident wave on the reflectarray aperture is proportional to their travel distance known as spatial phase delay. As a result, phasing components of the reflectarray must correct for this phase in order to create a collimated beam. Typical geometry of a planar reflectarray antenna with a feed antenna in a reflectarray coordinate system is shown in Figure 2.2 and the working mechanism is explained below as in [5].

$\Phi_{spd} = -kR_i$ gives the spatial phase delay of the ith element to the feed antenna, where R_i is the distance between the feed antenna and the ith element, and k is the wavemeter at the operating frequency. Similarly, the spatial phase delay of the center element is given by $\Phi_{spd0} = -kR_0$.

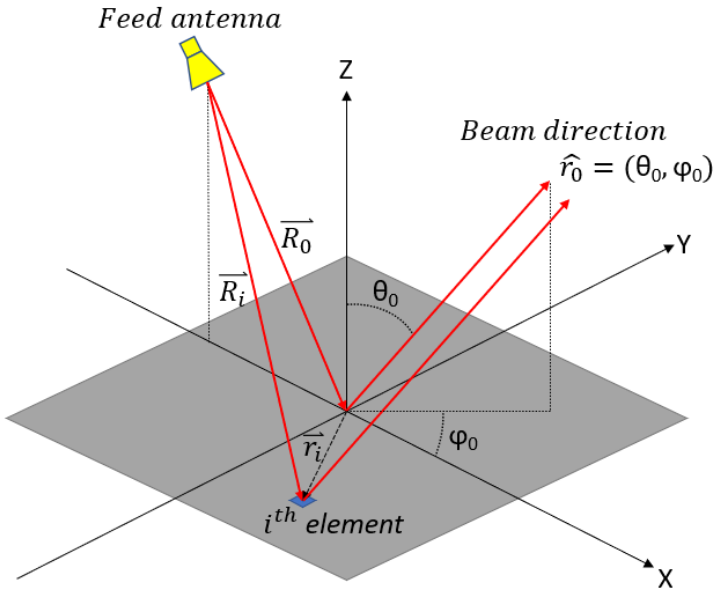

Figure 2.2: Geometrical parameters of a planar reflectarray antenna

In order to get a collimated beam in a certain direction, a progressive phase relative to the center element can be added to the aperture that the progressive phase difference between the ith and the center element is $\Phi_{pp} = -k\vec{r_i} \cdot \hat{r_0}$, where $\vec{r_i}$ is the space vector of the ith element and $\hat{r_0}$ is the direction of the collimated beam.

It clearly shows that a specific phase shift distribution on the reflectarray aperture is needed to compensate for the spatial delay and the progressive phase. So the equation can be listed as $\Phi_{spd} + \Phi_{rp} - \Phi_{pp} = \Phi_{spd0} + \Phi_0$ where Φ_{rp} is the phase shift of the ith element and Φ_0 is the phase shift of center element. Both sides of the equal sign represent phase delay of two different paths. In conclusion, phase shift required for each element on the reflectarray is given by

$$\Phi_{rp} = kR_i - kR_0 - k\vec{r_i} \cdot \hat{r_0} + \Phi_0 \ . \tag{2.1}$$

Once Φ_0, phase shift of the center element, is set to zero, phase shifts for all other elements can be calculated by

$$\Phi_{rp} = kR_i - kR_0 - k\vec{r_i} \cdot \hat{r_0} \ . \tag{2.2}$$

It's worth mentioning that the phase distribution calculated above will result in a pencil beam in the desired direction and other beam shapes can be achieved by changing the progressive phase part in the equation. In conclusion, reflectarray is similar to a parabolic

reflector antenna except the reflectarray has a fixed number of elements that are usually placed on a flat surface. As a result, the phase distribution on the reflectarray is basically pixelated.

2.2.2 phase tuning approaches

In the last section, phase shift on each element of reflectarray is proved to be essential for beam steering. To achieve aperture phase tuning in reflectarray systems, there are mainly three basic approaches: tunable delay lines, tunable patch size, and tunable rotation angles. Other novel approaches are also discussed in the following sections.

Tunable delay line

In the first approach, elements on the reflectarray transfer the incoming electromagnetic wave from the feed antenna into a guided wave along an attached transmission line with a certain length[6][7][8]. Either an open circuit or a short circuit can be used to terminate this transmission line based on the design technology used. The element re-radiates the signal after it reflects back from the transmission line termination. Typical reflectarray patches with delay lines of variable length are shown in Figure 2.3.

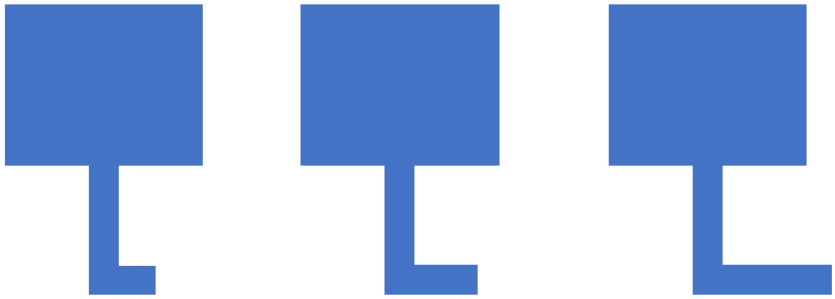

Figure 2.3: Reflectarray patches with delay lines of variable length

The wave radiated back from the open/short end has a phase shift proportional to twice the delay line length. So the phase difference required could be carried out by adjusting the line length. The first step is choosing suitable patch dimensions to make sure it resonates at a required frequency using the classic microstrip antenna analysis technique. The second step is perfectly matching the patch impedance to the delay line to allow maximum power delivering from the patch to the delay line and vice versa.

In reality, the linear relation between phase response and delay line length is distorted by other effects[9]. Firstly, the specular reflection from the ground plane will contribute to the total energy re-radiated from patches. Secondly, delay line resonance could occur at certain lengths. More importantly, unlike a single microstrip antenna, mutual coupling between two adjacent reflectarray elements should be considered during the design process.

Tunable patch size

The physical size of patches may be modified rather than adding delay lines since the length of a resonant element determines the antenna's resonance frequency, resulting in a different phase shift at a given frequency. In 1990, this method of phase tuning is first used over metallic patterns having a cross configuration with variable dimension[10]. Later, variable-sized rectangular patches and many other geometries like square and circular patches are also proven to be effective in phase tuning[11][12].

This approach has several advantages compared with the one using delay lines[13]. Firstly, an adaptation of delay lines with lengths of up to half a wavelength is no longer a concern in this approach. And the degradation of several electrical characteristics, such as dissipative losses and cross-polarization caused by bent delay lines is mitigated.

Because of the high Q factor feature of patch antennas, a minor change in the size of a resonating patch causes a broad range of phase changes in the reflected wave. Thus the phase change versus patch size is extremely non-linear due to the high sensitiveness near the resonance frequency which makes lower manufacturing tolerance errors and largely decreases the operating bandwidth of the reflectarray.

A thicker substrate can provide a smoother phase changing rate against the patch size by reducing the Q factor, but it introduces a smaller phase shift range[13]. Many other factors like mutual coupling effects and specular reflection from the ground plane also affect the reflection phase shift range.

Tunable rotation angles

This method of phase changing is restricted to co-polarization designs by rotating the elements which was first used in the reflectarray design in 1998[14]. When a co-polarization antenna element is rotated by φ, the radiation phase is changed by the same value. The advance or delay of phase is decided according to the direction of rotation[15]. The article[14] demonstrated a linear relationship between the phase shift of the reflected wave and the rotation angle. The mathematical formulation of this method is described here.

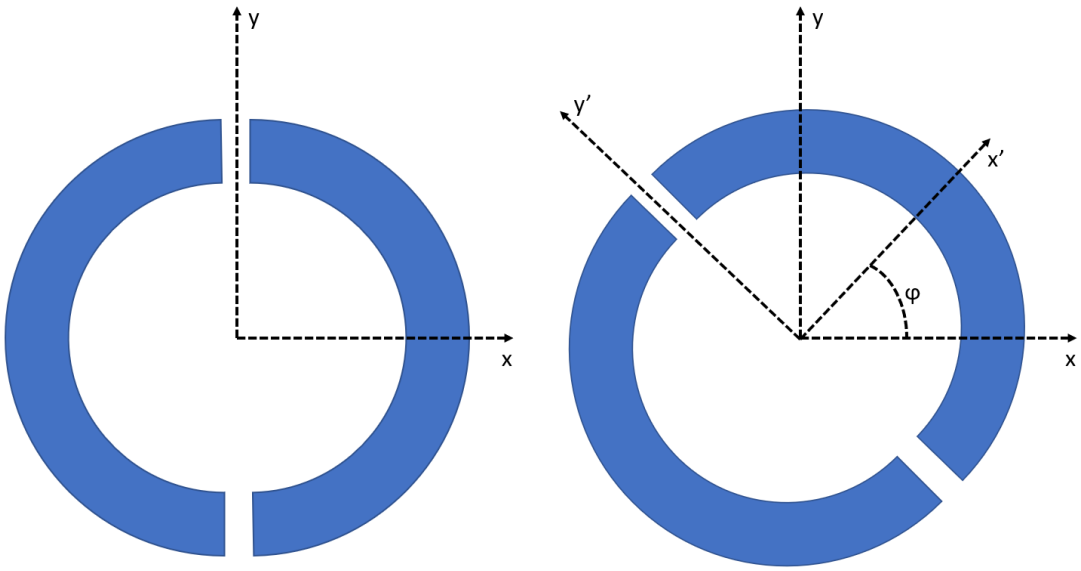

Figure 2.4: Circularly polarized reflectarray elements. Left: Original position; Right: rotated by φ

Supposing a right hand circularly polarized wave incidents in the -z direction on the element shown in Figure 2.4, it can be expressed by

$$\overrightarrow{E_i} = E_0(\widehat{u_x} + j\widehat{u_y})e^{jk_0z}e^{j\omega t}. \tag{2.3}$$

Normally, the reflected wave propagates in the $+z$ direction as a left hand circularly polarized wave and can be expressed as

$$\overrightarrow{E_r} = E_0(-\widehat{u_x}e^{j\phi_x} - j\widehat{u_y}e^{j\phi_y})e^{-jk_0z}e^{j\omega t}. \tag{2.4}$$

If the phase change in the y direction is leading by 180°, $\phi_y = \phi_x + 180°$, which can be achieved by split rings or attached delay lines, the reflected wave can be written as

$$\overrightarrow{E_r} = E_0(-\widehat{u_x} + j\widehat{u_y})e^{j\phi_x}e^{-jk_0z}e^{j\omega t}. \tag{2.5}$$

If the element is rotated by φ, the incident wave in this new coordinate system becomes (x', y') can be expressed in the form of

$$\overrightarrow{E_i}' = E_0[(\overrightarrow{u_{x'}}cos\varphi - \overrightarrow{u_{y'}}sin\varphi) + j(\overrightarrow{u_{x'}}sin\varphi + \overrightarrow{u_{y'}}cos\varphi)]e^{jk_0z}e^{j\omega t} \tag{2.6}$$

which can be simplified as

$$\overrightarrow{E_i}' = E_0(\widehat{u_{x'}} + j\widehat{u_{y'}})e^{j\varphi}e^{jk_0z}e^{j\omega t}. \tag{2.7}$$

The reflected wave in this situation is given by

$$\overrightarrow{E_r}' = E_0(-\widehat{u_{x'}} + j\widehat{u_{y'}})e^{j\phi_{x'}}e^{j\varphi}e^{-jk_0z}e^{j\omega t}. \tag{2.8}$$

It should be noticed that the element is symmetric with rotation which results in $\phi_x = \phi_{x'}$ and $\phi_y = \phi_{y'}$. So after the reflected wave expression is reorganized in the original coordinate system,(x, y), it is given by

$$\overrightarrow{E_r} = E_0(-(\overrightarrow{u_x}cos\varphi + j\overrightarrow{u_y}sin\varphi) + j(-\overrightarrow{u_x}sin\varphi + j\overrightarrow{u_y}cos\varphi))e^{j\phi_x}e^{j\varphi}e^{-jk_0z}e^{j\omega t}, \tag{2.9}$$

and still can be simplified as

$$\overrightarrow{E_r} = E_0(-\widehat{u_x} + j\widehat{u_y})e^{2\varphi}e^{j\phi_x}e^{-jk_0z}e^{j\omega t}. \tag{2.10}$$

When comparing the reflected wave expressions of the original and rotation situations, it is evident that if the element is rotated counterclockwise by φ, the reflection phase is delayed by 2φ.

In the analysis above, the reflection loss and cross-polarized reflection field are assumed to be zero which will influence the performance of practical designs.

Other approaches

The ideas using delay lines and variable-sized patches are all based on the principle that phase shift happens at a certain frequency when the resonance frequency of the reflectarray element shifts. A well-known method of changing resonance frequency is employing varactors. Varactor diodes were first used in reflectarray beam-steering antenna in 2002[16]. Different schemes of the elements arrangement were discovered to increase the phase shift range of reflectarray with varactor diodes that are shown in Figure 2.5[17][18][19]. And the varactor diodes can be replaced by micro electrical-mechanical systems(MEMS) varactors for the same purpose[20][21].

Moreover, these methods can be thought of as manipulating the effective length of the resonator which means many other MEMS designs can be implemented other than MEMS varactors. For example, slotted patches loaded with MEMS switches are used for

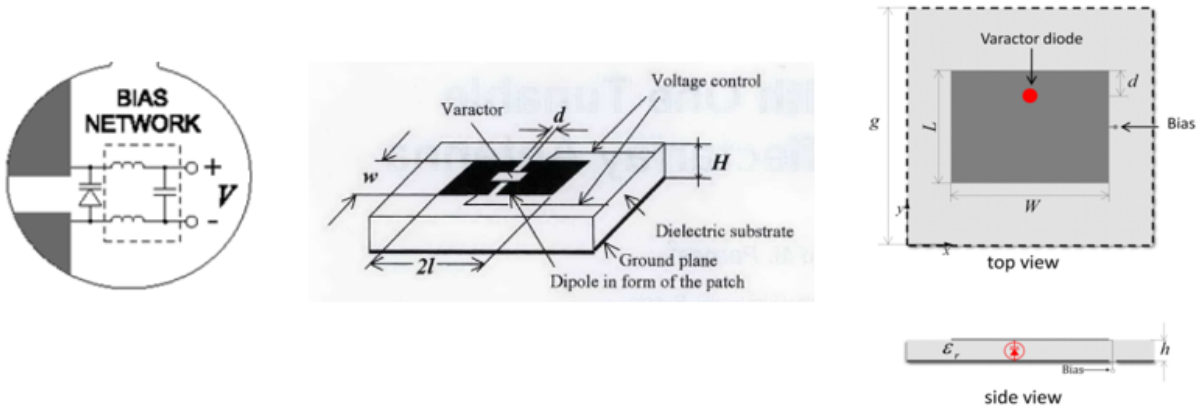

Figure 2.5: Reflectarray schemes using varactor diodes[17][18][19].

re-configurable reflectarrays[22][23]. Discontinuity planes in multiple planar sub-domains of various scale levels are also able to provide phase shift and the switches between are used for tunability[24][25].

The resonance frequency of a reflectarray element can be also tuned by changing the dielectric constant of the substrate material. A typical material with variable properties is liquid crystal whose dielectric constant varies when different biasing voltages applied. It has been used in many reflectarray applications[26][27][28][29] with an essential disadvantage of liquid crystal cannot be ignored that it takes a relatively long time for chiral phase of liquid crystal molecules to return to a disordered state. The bandwidth performance also limits the applications of liquid crystal. Another material employed in the reflectarray antenna is Ferro-electric films[30][31].

2.2.3 Applications

As previously discussed, the reflectarray antenna includes many of the key advantages of both classic parabolic reflector and microstrip patch antenna. It has been used in many recent applications and can be implemented in possible future applications.

Beam steering/scanning

One of the key applications of reflectarray is beam steering/scanning by manipulating the resonance frequency of the resonator on each element or mechanically tilting the whole

array instead.

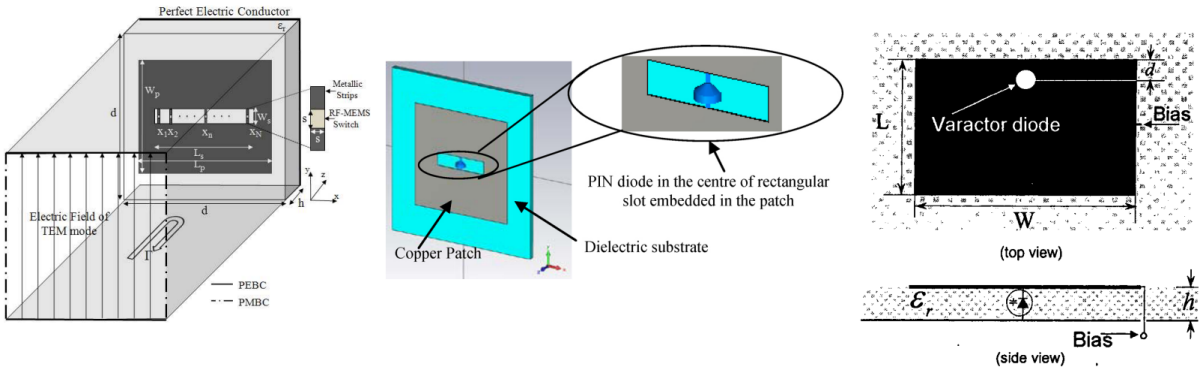

Figure 2.6: Beam steering reflectarray using RF MEMS, PIN diodes or varactors[32][33][35].

A beam steering reflectarray antenna using the first method can be viewed as a phased array where phase shifters are directly attached to the antenna elements so that reflectarray antenna has lower insertion loss. Figure 2.6 shows that the so-called phase shifters can be achieved by RF MEMS[23][32], PIN diodes as switches[33] or employing varactor diodes to vary the capacitance of the resonant elements[34][35]. The feed antenna is out of reflectarray, hence, there is no need for complex power division circuitry or expensive transmit/receive modules.

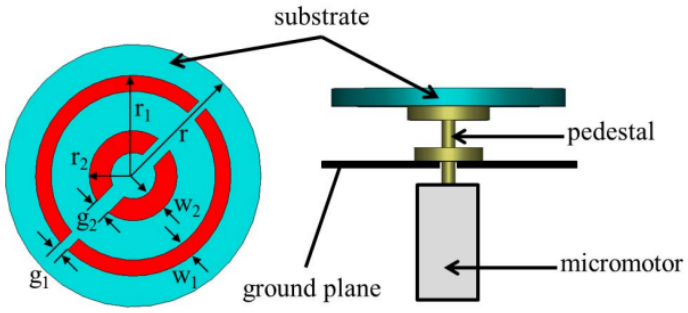

Figure 2.7: A reflectarray element with a motor on the backside[36].

Some beam steering reflectarrays use micro motors or actuators for mechanical control of each individual reflectarray element to avoid any insertion loss brought by phase shifters[36][37][38] as Figure 2.7 depicted. Motors or actuators are attached on the backside of each element with an ability of 180° rotation and a 360° phase changing range. Because

the reflectarray typically has a significant number of components, efficient control, and design complexity of a big number of motors is required. To solve the problem, actuators allowing the array moves as a whole are implemented in beam steering reflectarray[39][40] like Figure 2.8 shows. The phase changing ranges of this method is twice the tilting angle of the array plane and the pattern of the element needs to be carefully designed to minimize the mutual coupling between adjacent elements.

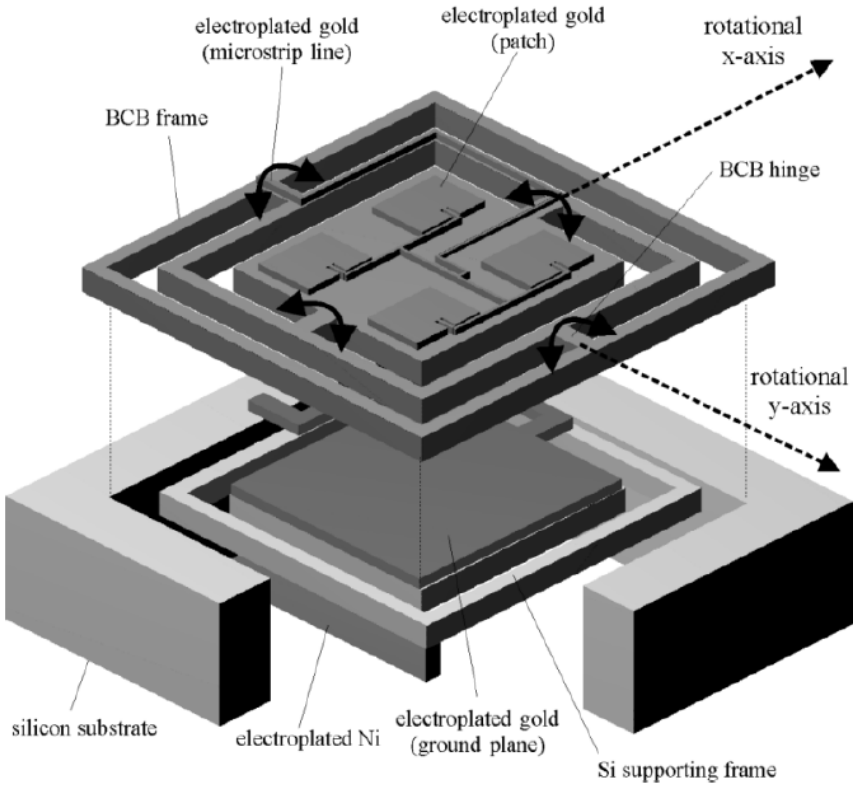

Figure 2.8: A 2-D beam steering array[40].

Power amplifying and combining

Besides serving as a passive reflectarray antenna, active components can be integrated into a reflectarray unit and then used for power amplifying and combining which has been proven by Bialkowski of the University of Queensland, Australia[41][42][43].

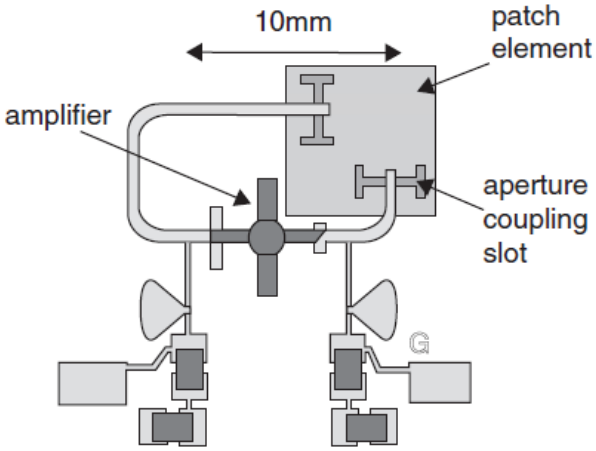

Figure 2.9: A reflectarray element for power amplifying[41].

In [41], an X band amplifying reflectarray antenna was initially demonstrated. Each reflectarray element is designed employing transistors as shown in Figure 2.9. This configuration uses a dual-feed, single aperture coupled microstrip patch allowing for minimal dimensions of the transistors and related matching networks so that it provides enough isolation between the two antenna feeds to avoid oscillations. Plane-wave with one polarization from a horn antenna placed in the space radiates on every patch on the reflectarray. Signals received from patch elements are sent to an amplifier via slots on the ground layer and then re-radiates out into space from its orthogonal port. The different phase shift of each element was achieved by adjusting the length of the transmission line between the two slots.

A spatial power combining antenna was discussed in [43]. It consists of an amplifying reflectarray and a feed transmitting/receiving sub-array as shown in Figure 2.10. In practice, an orthomode horn antenna can replace the feed sub-array. The two arrays in this design use identical dual-feed aperture coupled patches as radiating elements. Figure 2.11 displays that the feed sub-array has four patches with both transmitting and receiving capabilities. Waves illuminate on the feed sub-array and are re-transmitted to the other reflectarray. During that process, the polarization is changed from vertical to horizontal and the signals re-radiate back the feed sub-array after amplification. To achieve the power combining ability, multiple feeds should be used and placed at certain locations with respect to operating frequencies. The phase shift of each element also has to be carefully configured to combine the power into a single radiation beam.

The power amplifying and combining reflectarray has several advantages. Firstly, it

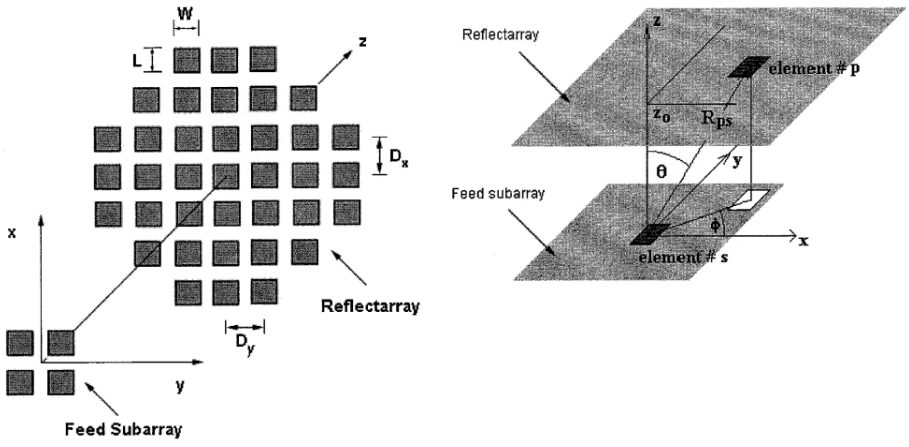

Figure 2.10: A feed sub-array and a receiving reflectarray[43].

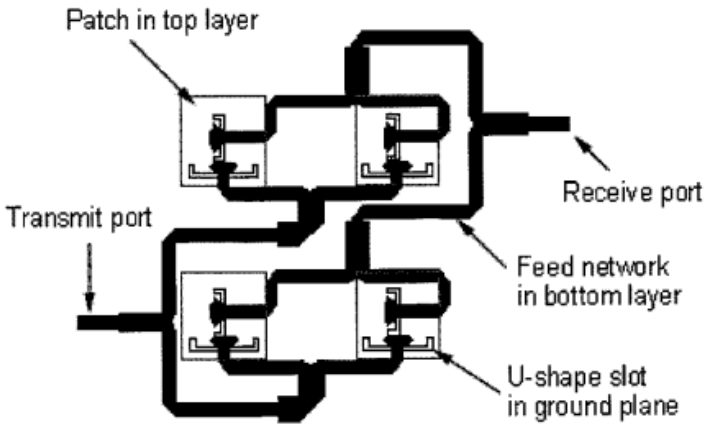

Figure 2.11: A feed array with four patches with transmitting and receiving capabilities[43].

increases the overall gain of the antenna. Secondly, at high frequencies, transistor sizes are very small which requires a power combining function to increase output power. Losses in transmission line based power combining circuits will be considerably low while using spatial power combiners.

Very large aperture applications

A large aperture antenna is one of the few solutions for long-distance communications with a high data rate and fine radar imaging resolution due to mechanical advantages and low power loss. Many different planar and conformal geometries can be adopted for a large number of potential applications.

For example, NASA's Earth remote sensing and deep space exploration programs employed a planar reflectarray using an inflatable structure and thin membrane. The advantages compared to parabolic reflectors are very low mass and small storage volume. While side effect of the increasing electrical sizes is the limited bandwidth which still exists using the multiple-stacked-patch approach. One possible method is using many small pieces of reflectarray on a parabolic surface[44]. The curved surface for reflectarray can provide two benefits. The first one is the incident angles from the feed antenna to the elements are minimized so that the radiation efficiency for each element is relatively higher and more constant. The second one is reducing the phase delay differences between the feed antenna and elements. The reason for using many small flat reflectarrays instead of a reflector antenna is it allows easy mechanically folding of the flat panels into a small structure for the precious space storage volume.

A more aspiring idea is to use reflectarrays in solar sails[45]. The difficult part is how to collect enough solar flux power to provide thrust for spacecraft. Besides, large aperture reflectarrays can be also used in various ground applications like radio telescopes and solar power facilities.

2.3 Metasurface

2.3.1 Definitions and characteristics

Before getting into metasurfaces, there is one concept that needs to be introduced, metamaterial. Metamaterial receives its so-called name because it's a kind of novel artificial

synthetic material engineered to achieve unique properties which cannot be found in nature. The dimension, density, shape, and orientation of inclusions are able to be controlled to fulfill the designer's requirements.

It's a fact that phase response reverses as frequency varies around the resonance frequency when resonances happen[46]. If each element of such material is resonant, it can achieve negative values for both effective relative permittivity and permeability. A negative refractive index is also possible with this kind of material in the optical field. So it's also called double negative media (DNG), left-handed media, and backward wave media in some literature[47][48][49].

The normal structure of metamaterials consists of a few small scatterers such as metallic rings, metallic rods, or spherical magneto-dielectric particles in an array within a region of space[50]. Thus, problems such as manufacturing complexity, bulkiness, losses, frequency range, scalability, and disperses occur due to their 3D nature and resonant properties[51]. This idea of metamaterial may be further developed by strategically arranging electrically small scatterers in a two-dimensional pattern on a surface or interface that is called metasurface[52]. First, metasurfaces are easy to fabricate and implement. A negative refraction index can still be provided by the phase discontinuity across the metasurface, which preserves the excellent metamaterial capabilities[53]. Second, the functioning of bulky metamaterials needs fairly large distances for wave propagation and therefore the performance of metamaterial applications will decay in intrinsic losses and bring accompanying resonances. Finally, due to the exceedingly thin layers, metasurfaces are allowed to be integrated into nanophotonic systems and provide many solutions for novel antenna designs in the microwave field[54].

The metasurface is not a new idea brought for a 2-D structure guiding electromagnetic waves. The frequency-selective surfaces (FSS) were developed as spatial filters[55][56]. The reflectarray antennas mentioned in the previous section developed as flat equivalents of parabolic reflectors. The transmitarrays are the transmissive equivalents of the reflectarrays. All of them are the pioneers of modern metasurfaces.

Metasurfaces are characterized as periodic or non-periodic structures with small individual element thickness and periodicity compared to the operating wavelength[51]. Or Metasurfaces are defined as a symmetric or asymmetric array of sub-wavelength resonant scatterers that decide the surface's electromagnetic response based on the distribution of each scatter on the array[57]. This is the main difference between metasurfaces and FSS because periodicity in a typical FSS is half of the operating wavelength. Another difference is brought by the sub-wavelength structures which can be viewed as a homogeneous structure or a circuit made of lumped elements[58]. A general method to analyze the meta-

surfaces is replacing the complex distribution of elements with perfect electric conductor (PEC) and perfect magnetic conductor (PMC) boundary conditions[59]. Metasurfaces with non-periodic arrangements of elements can be viewed as reflectarrays mentioned in section 2.2.

For difficulties of wave propagation at the far-field limit as well as near-field diffraction and reflection, the Huygens–Fresnel principle applies. It says that every point on a wavefront is a source of spherical wavelets and the secondary wavelets emitted by different points interfere with each other. The wavefront is formed by adding these spherical wavelets thus the wavefront can be controlled beyond the source itself by adjusting each point source. In metasurfaces, electric and magnetic dipole moments are triggered when an electromagnetic wave hits the surface and then the dipole moments are transformed to surface current[60]. According to the surface equivalence principle, surface currents are equal to the tangential electric and magnetic fields which decide the reflection response of a surface.

2.3.2 Applications

Surface patterns interact with electromagnetic waves, resulting in a phase discontinuity across the metasurface. The surface currents can lead or lag depending on every resonant element since all elements on a metasurface can be spatially changed. This localized phenomenon allows us to customize wavefronts as they travel through or are reflected back from a metasurface, which opens up a wide range of applications with the advantage of less bulkiness than a 3-D metamaterial structure. A few possible operations of metasurfaces are schematically concluded by Glybovski as shown in Figure 2.12 [58].

Wavefront shaping

The usage of reflectarrays and transmitarrays in beam steering, which is similar to wavefront shaping, is described in section 2.2. This function is achieved by the implementation of tunable delay lines, tunable patch size, tunable rotation angles, or varactor diodes. However, due to the periodicity of the order of half a wavelength, such reflectarrays or transmitarrays do not offer sub-wavelength resolution which is critical for aperture efficiency. Normally the homogenization theory is not suitable for the analysis of such arrays and they cannot be categorized as metasurfaces.

The local phase response of metasurfaces, which gradually changes along with the surface coordinates, could be explained in terms of induced electric and magnetic aver-

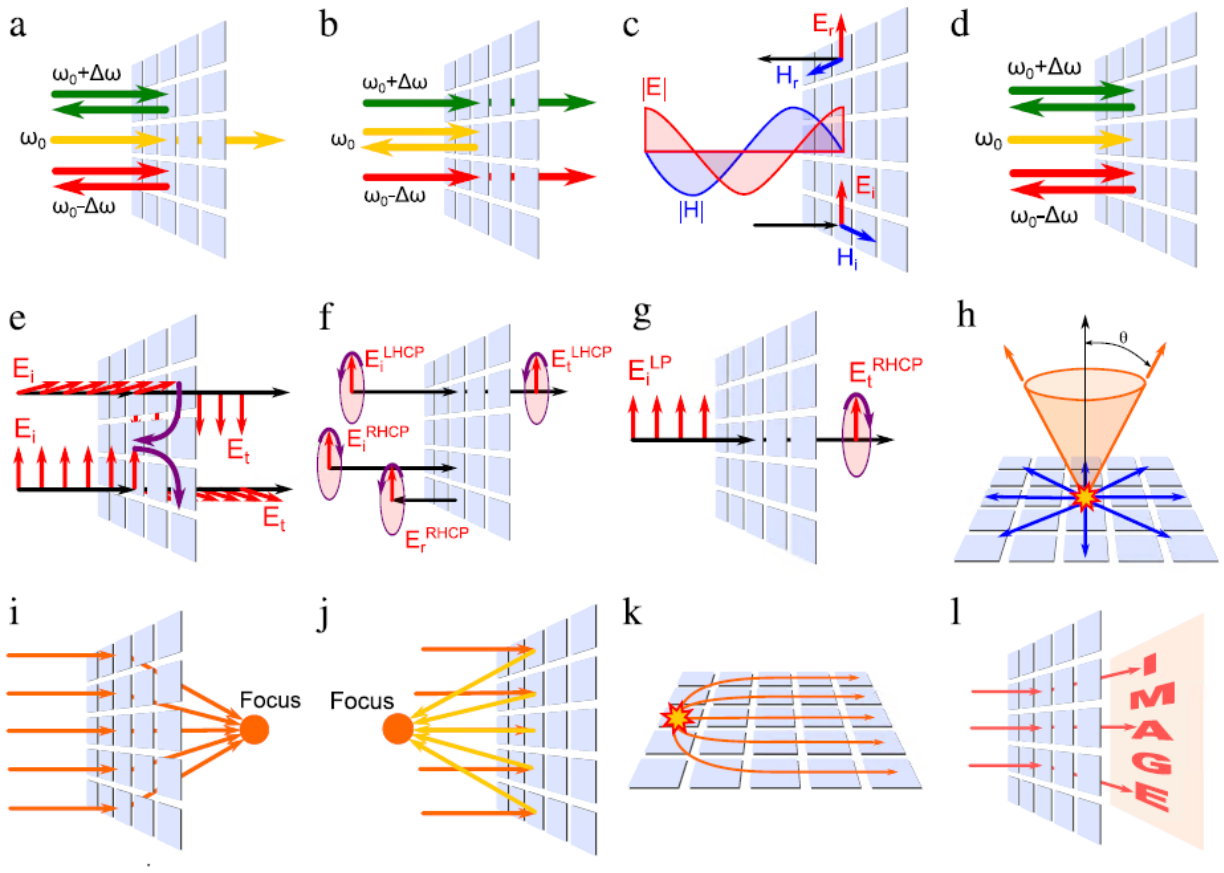

Figure 2.12: Possible operations of metasurfaces: (a) bandpass frequency selective surface; (b) bandstop frequency selective surface; (c) High-impedance surface; (d) narrow band perfect absorber; (e) twist polarizer; (f) right-handed circular-polarization frequency selective surface. (g) linear-to-circular polarization converter; (h) 2-D leaky-wave antenna; (i) Focusing transmitarray; (j) Focusing reflectarray; (k) flat Luneburg lens; (l) hologram.[58]

aged surface currents owing to their sub-wavelength dimensions[58]. The reflecting and transmitting phased metasurfaces may be thought of as nonuniform electric and magnetic current sheets if the entire structure's thickness and periodicity are both sub-wavelength. By replacing the traditional reflectarray of near-resonant patches with an impedance metasurface consisting of sub-wavelength patches on a grounded dielectric substrate, wave-front modifying metasurfaces were obtained.

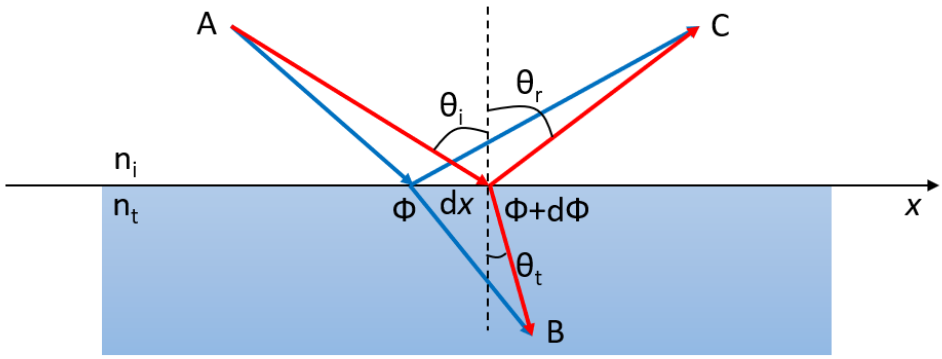

Figure 2.13: Schematic diagram of generalized Snell's Law based on Fermat's principle[61]

Design of reflectarray-like or transmitarray-like metasurfaces can be achieved by a generalized Snell's law based on Fermat's Principle as depicted in Figure 2.13 [61]. The relations between incident angle, reflection angle, and refraction angle are

$$n_t sin\theta_t - n_i sin\theta_i = \frac{\lambda_0}{2\pi}\frac{d\phi}{dx}, \tag{2.11}$$

$$sin\theta_r - sin\theta_i = \frac{\lambda_0}{2\pi n_i}\frac{d\phi}{dx}, \tag{2.12}$$

where n_i and n_t are refraction indices of two homogeneous materials that hold a metasurface in the interface plane, $\phi = \phi(x)$ is the designed phase variation along with the x-axis of a metasurface and λ_0 is the free-space wavelength.

A whole range of 360° reflection or transmission phase changing range is mandatory for wavefront shaping of metasurfaces. The local phase manipulation of metasurfaces can be achieved by many approaches. Varying the size of square patches on a dielectric layer with a ground plane was demonstrated to be effective in wavefront shaping[62]. A birefringent metasurface has been successfully produced by regulating the size and response of each subwavelength inclusion along both perpendicular axes[63]. In the terahertz range, a similar

technique utilizing perpendicular strip dipoles in a triangular lattice was published in [64]. Using multiple heterogeneous layers, another approach for replicating the behavior of any material has been created[65]. A series of artificial cylindrical dielectric samples with a variety of relative permittivities and loss tangents at microwave frequencies were created by altering the weight proportion of various materials.

Frequency selective surfaces

Spectral filtering is one of the most common operations in signal processing networks, both in the microwave and optical areas. Frequency selective surfaces (FSS) provide such functionality for electromagnetic waves propagating in homogeneous media. A typical frequency selective surface is a periodic structure designed to work at the resonance frequency with a periodicity of half a wavelength. Metasurfaces are a good replacement for frequency selective surfaces owing to their similar nature.

As mentioned in previous sections, a metasurface works with a periodicity of subwavelength thus bringing many advantages in comparison with traditional frequency selective surfaces. The smaller periodicity of metasurface allows a larger amount of unit cells in the same space which is beneficial in most cases[66]. FSS metasurfaces also exhibit a steady reaction to variations in the incidence angle of the electromagnetic wave due to the tiny size of the unit cell[67]. Resonant dipole and slot structures are fully used to form an LC resonant structure with a resonant frequency smaller than the wavelength. In addition to novel structures, the dimension of a unit cell of periodic metasurfaces has been also reduced using lumped elements such as capacitors[68], convoluted elements[69], split-ring resonators[70], and other non-reciprocal bianisotropic elements[71].

Another issue with FSS metasurfaces is obtaining the proper dispersion characteristics, which can be more difficult than a first-order resonance curve, such as dual-band filtering. Combining two complimentary patterns with the same periodicity into one unit cell, generally by printing their metallic parts on opposite sides of a dielectric layer, is one of the available techniques to achieve dual-band filtering[72]. Another method is putting two resonating structures with the same shape but different dimensions inside the same unit[73]. The patterns used in these two methods are shown in Figure 2.14.

High-impedance surfaces

Many applications require directed radiation from an omnidirectional feed. High-reflective mirrors or wire meshes are the traditional options that can provide a reflection coefficient

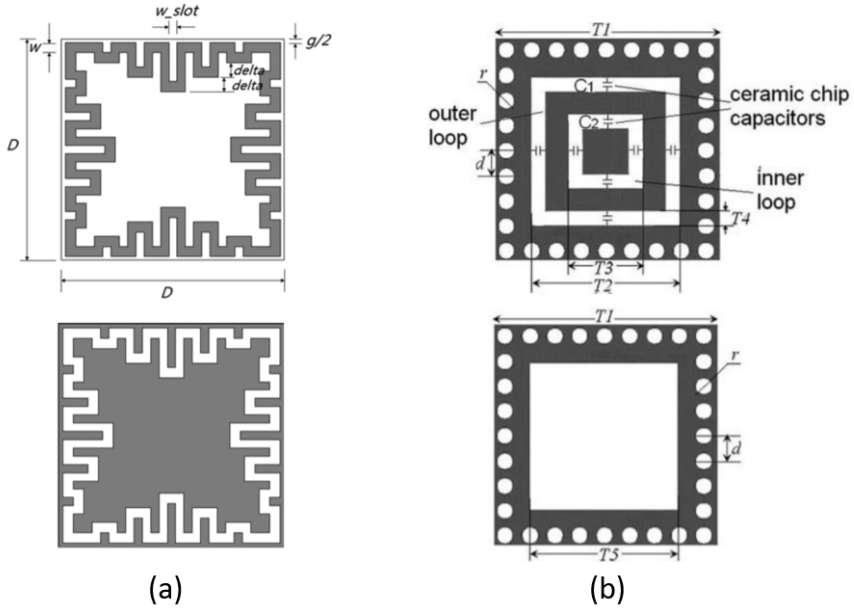

Figure 2.14: Two methods of dual band filtering metasurfaces.(a) complementary patterns[72]; (b) patterns with the same shape but different dimensions[73].

close to -1[74]. However, if the distance between the feed and the reflectors is too small compared with the wavelength, radiation efficiency becomes considerably low. From an impedance matching point of view, PEC reflectors at a quarter-wavelength distance to the feed provide the best reflection performance, while this distance could be intolerable in some applications.

The first possible solution is placing the feed on top of a grounded dielectric layer with a thickness of $\lambda_d/4$, where $\lambda_d/4$ is the wavelength in the dielectric media, to fully use the nature of high permittivity of dielectric material that could relatively reduce the distance requirement. But the shortcoming of this method is a lower radiation gain due to the induced current on the ground layer of the other side of the dielectric[75].

Metasurfaces used for solving this problem in the microwave field are known as high-impedance surfaces[76]. It's a two-dimensional array used to fully reflect an incident plane wave in phase with a sub-wavelength periodicity which means there is a linear relationship between the averaged tangential components of electric and magnetic fields as in the following Equation 2.13.

$$Z_s \vec{n}_0 \times \vec{H}(z=0) = \vec{E}(z=0) \tag{2.13}$$

The tangential component of the magnetic field can be seen as zero when the impedance is high enough, and the reflection coefficient is +1. This means the induced surface electric currents are zero and there are only non-zero magnetic surface currents contributed to reflected waves according to the surface equivalence principle. Such surfaces serve as perfect magnetic conductors (PMC).

There are various approaches to achieving high impedance surfaces in the literature. A mushroom surface was brought in [76] which was analyzed in the form of a parallel resonant circuit. The capacitance comes from fringing fields between edges of adjacent patches and the inductance appears due to the current loop flowing around the path from patches and ground. A high impedance surface made of dipole array over a grounded dielectric media was produced with a similar equivalent circuit in [77].

Tunable metasurfaces

Since metasurface response is based on localized control, tunable metasurfaces can be realized and fulfill a wide range of applications. Similar to tunable reflectarrays, there are several approaches: mechanical tuning, use of varactors, and manipulation of material characteristics. Mechanical tuning has been brought by rotating individual elements[78]. MEMS structures are very useful in tunable metasurfaces as they are able to provide tilt, tip, or piston movements[79]. Varactor diodes can be also easily integrated into tunable metasurfaces as the capacitance can be controlled by DC voltage across anode and cathode[59][80]. In [81], metasurfaces with dispersive refractive index have been proposed for the THz domain. The structures mentioned above are shown in Figure 2.15.

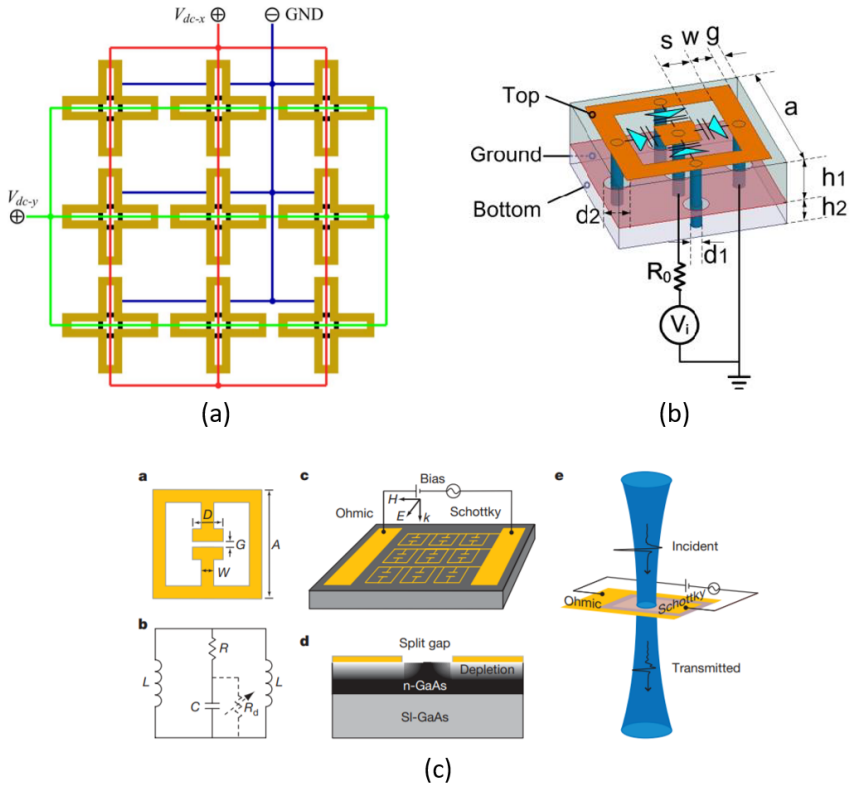

Figure 2.15: Three approaches of tunable metasurfaces.(a) Mechanical tuning[79]; (b) Varactor diodes[59]; (c) Dielectric characteristic manipulation[81].

Chapter 3

Design and Simulation

As presented in Chapter 2, both metasurfaces and reflectarrays could be employed to form a collimated beam in the desired direction by adjusting the reflection phase. The two most important portions to achieve that goal are phase distribution calculation and phase shift simulation of each element. Section 3.1 discusses how to arrange the reflection phase of each unit on board using MATLAB, based on spatial phase delay and desired beam direction. Section 3.2 provides two types of tunable metasurfaces. The phase shift could be achieved either by inserting varactors between each element or by rotating the reflecting plates. In section 3.3, two types of tunable reflectarrays are introduced. Varactors are used in the first type to change the phase of the reflected wave. A phase shift can be also realized by the mechanical movement of central plates on each element in the reflectarray. The main work of sections 3.2 and 3.3 is done in Ansys HFSS 2020R2 to find the best structures to realize sufficient phase shift range.

3.1 Phase distribution calculation

Phase distribution directly decides the shape and direction of the reflected beam. As mentioned in Chapter 2, the equation for phase shift needed for each element is

$$\Phi_{rp} = kR_i - kR_0 - k\vec{r_i} \cdot \widehat{r_0} + \Phi_0. \tag{3.1}$$

The MATLAB codes for phase distribution calculation based on this equation are attached in Appendix A. The following is an example of how it works. The layout of a reflectarray with a square aperture operating at 3.5 GHz is given in Figure 3.1. Each

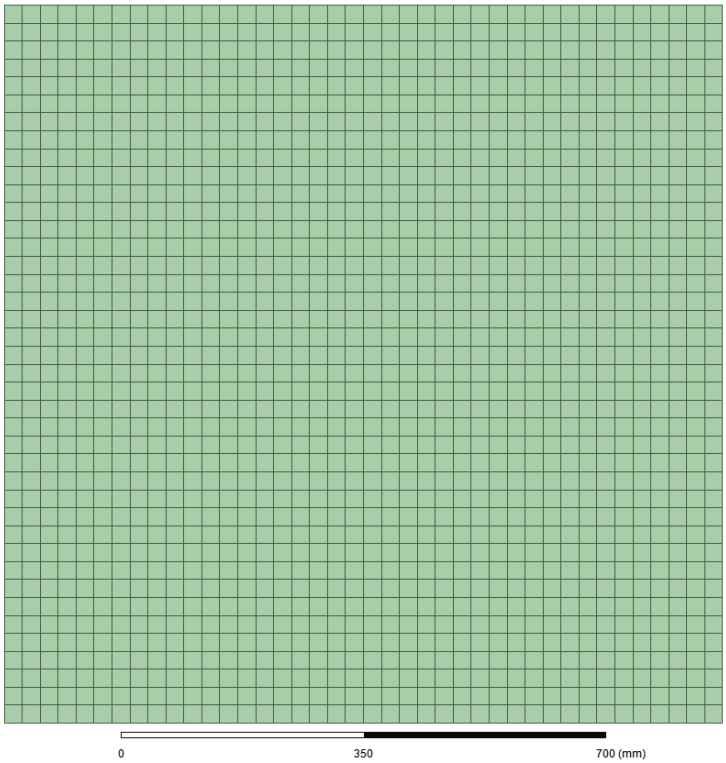

Figure 3.1: Layout of a reflectarray with square aperture.

block represents an element with a constant phase over its own aperture. The side length of this reflectarray is 1.04 m and the element spacing is 26 mm, giving 1600 elements in total for this array. Figure 3.2 shows a feed antenna placed above the array at the position (-0.01 m, 0 m, 1.00 m), which is slightly deviated from the Z-axis.

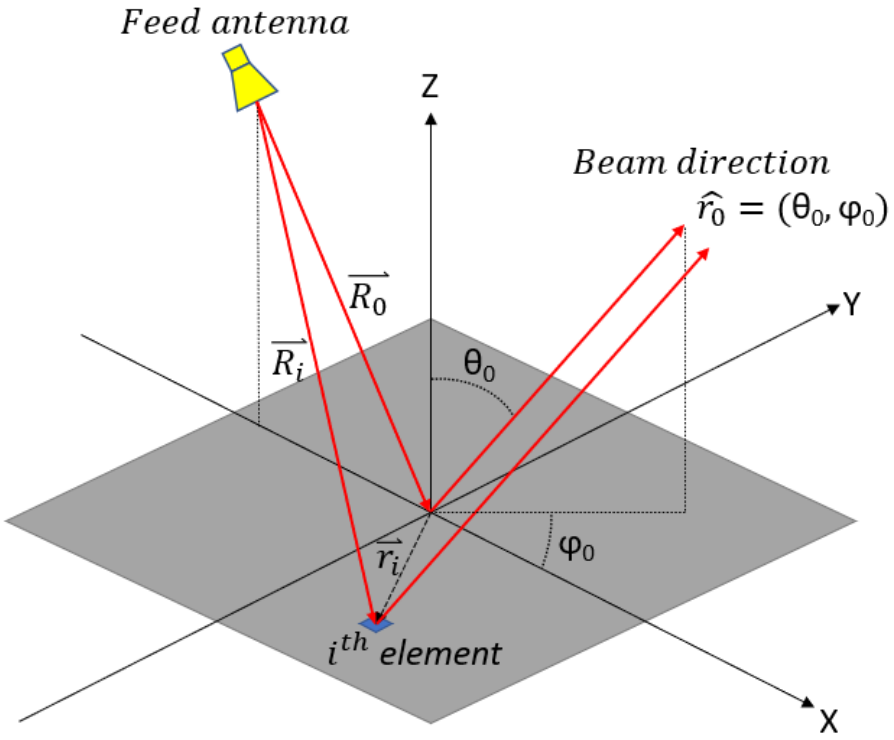

Figure 3.2: Geometrical parameters of a planar reflectarray.

When a reflected beam direction is confirmed, phase distributions are automatically generated in MATLAB. The phase distribution for when a reflectarray provides a broadside beam ($\theta_0 = 0$, $\phi_0 = 0$) is illustrated in Figure 3.3, which clearly shows a phase range from 0° to 360°. Phase distribution assuming different beam angles is plotted in Figure 3.4,

As mentioned in Chapter 2, three options are available to achieve aperture phase tuning: either extra phase delay is added to each element, or the aperture size of each element is changed, or electrical tuning is introduced. In sections 3.2 and 3.3, two methods for changing the reflection phase of both metasurfaces and reflectarrays are simulated.

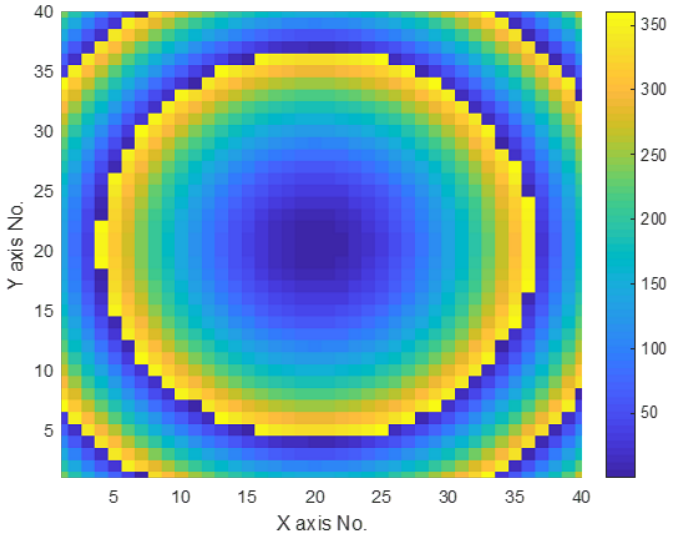

Figure 3.3: Phase distribution when a broadside beam is reflected.

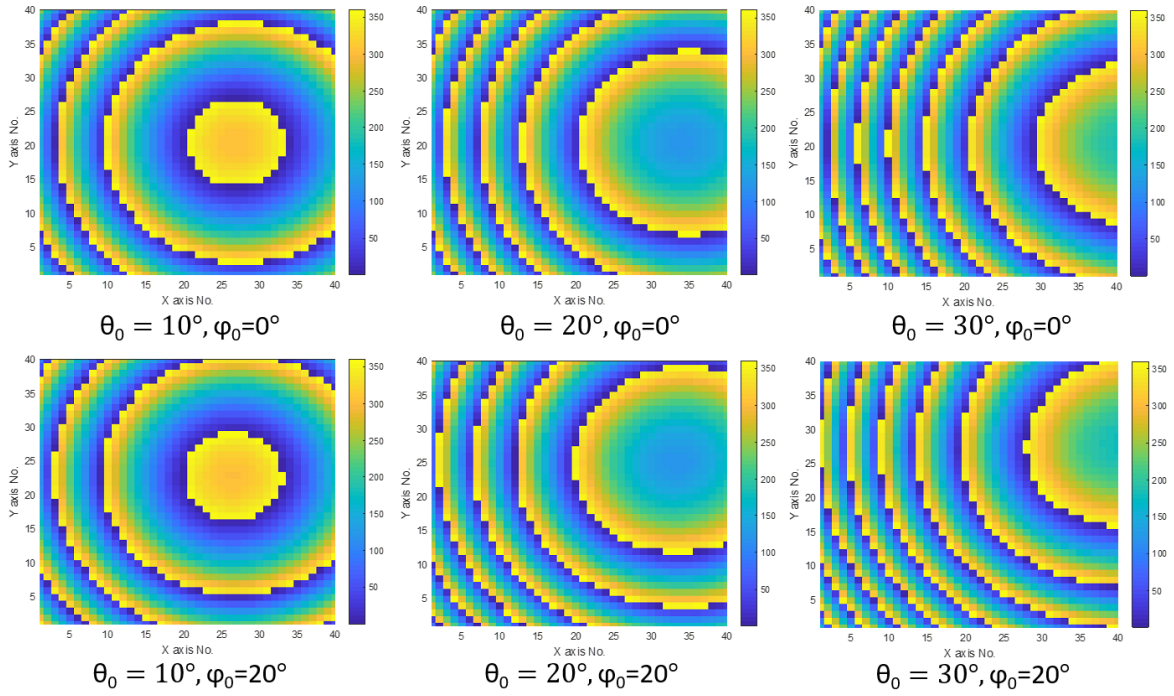

Figure 3.4: Phase distribution assuming different beam angles.

3.2 Tunable metasurface

In this section, a metasurface with the mushroom structure mentioned in Dan Sievenpiper's article [76] is discussed. It is a two-layer surface with pillars connected in between, as shown in Figure 3.5. Although only a two-by-two array is shown in Figure 3.5, the finite-element model analysis is employed in Ansys HFSS 2020R2 to characterize the reflection of each unit in a periodic array. Primary/secondary boundary conditions are applied to each unit.

According to $f = \frac{1}{2\pi\sqrt{LC}}$, the resonance frequency and reflection phase of a resonator can be shifted by changing the capacitance or the inductance. The inductance is fixed, because it is determined by the distance between the two metal layers. Two methods for changing capacitance are presented below.

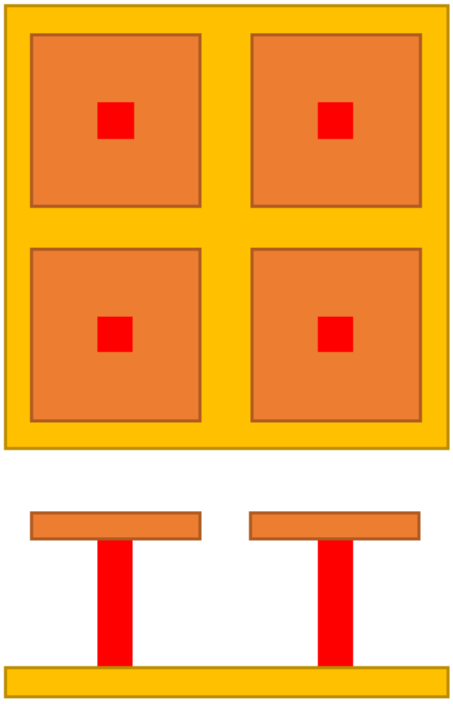

Figure 3.5: Top and side views of metasurface.

3.2.1 Electrically tunable metasurface

The first mechanism for changing a capacitance is by inserting a varactor between every two adjacent top patches [82].

The structure in Figure 3.6 consists of a two-by-two array with a period of 10 mm and a gap between the patches of 0.8 mm. The distance between the top patch and the bottom layer is 1.6 mm. The top boundary of the model box is set to floquet port and the four side boundaries are set to primary/secondary boundary conditions. The capacitors are built-in lumped models in Ansys HFSS 2020R2 and are set to the same value.

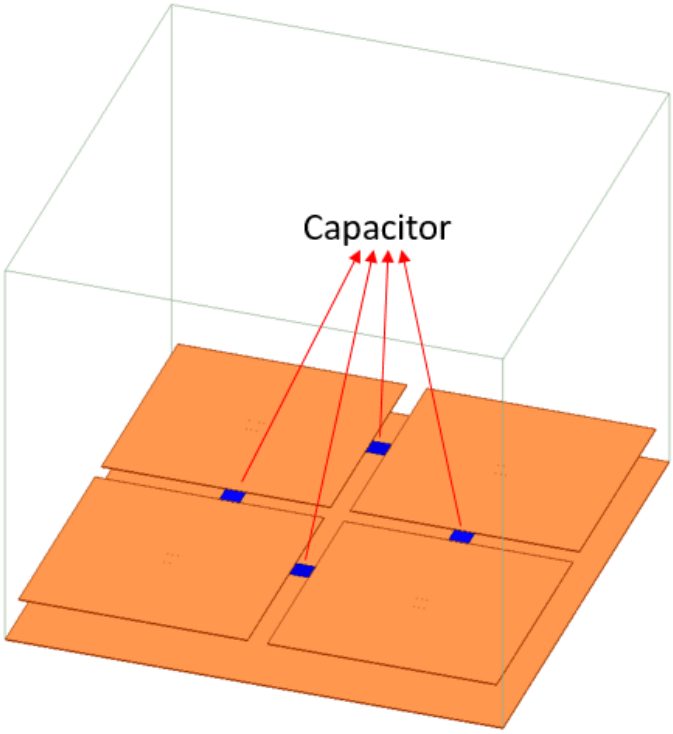

Figure 3.6: Two-by-two metasurface with capacitors between patches.

By running a parametric sweep, the capacitance can be changed from 0.1 pF to 0.8 pF. The magnitude and phase of reflection coefficient as a function of capacitance and frequency are shown in Figure 3.7.

The resonance frequency changes from 4.8 GHz to 2.7 GHz correspond to a capacitance from 0.1 pF to 0.8 pF. The phase shift range covers a full tuning range.

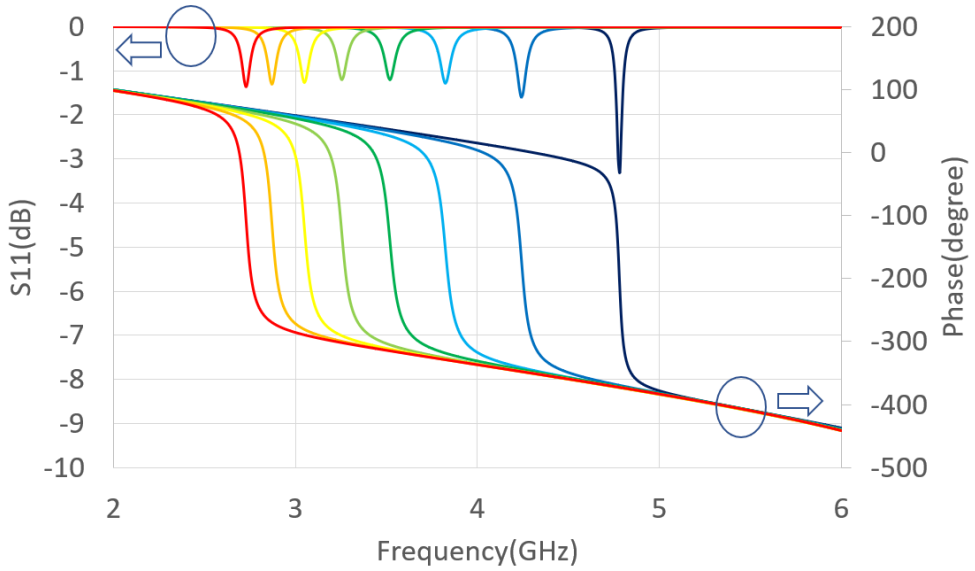

Figure 3.7: Magnitude and phase of reflection coefficient of a metasurface with varactors. From left to right: 0.8 pF, 0.7 pF, 0.6 pF, 0.5 pF, 0.4 pF, 0.3 pF, 0.2 pF, and 0.1 pF.

3.2.2 Mechanically tunable metasurface

The second mechanism for changing the capacitance is by tilting top patches and forming variable overlap areas, i.e., effective variable capacitors. The structure shown in Figure 3.8 is similar to the electrically tunable metasurface except with the patches on top being tilted.

The mechanism of the tuning capacitance is displayed in Figure 3.9. L is the length of the patch, g is the gap between adjacent patches when there is no tilt, and d is the distance between two parallel patches when there is an overlap area with a tilt angle of θ. The overlap area $A = [L - (L + g)cos\theta] \times L$ and the patch distance $d = (L + g)sin\theta$. Thus, the capacitance formed from the overlap area can be calculated by $C = \frac{\epsilon_0 A}{d}$. It can be clearly seen that a smaller gap g leads to a larger overlap area, and that a large distance th between patches and bottom layers leaves more space for the tilt. $L = 9.8\ mm$, $g = 0.2\ mm$ and $th = 4\ mm$ are chosen in the simulation.

The capacitance of the overlap area is calculated in MATLAB, as plotted in Figure 3.10. The capacitance increases from 1 fF to 20 fF as the tilt angle changes from 12 *degrees* to 30 *degrees*. Calculation of the capacitance starts from 12 *degrees*, because there is no overlap with a smaller tilt angle than that.

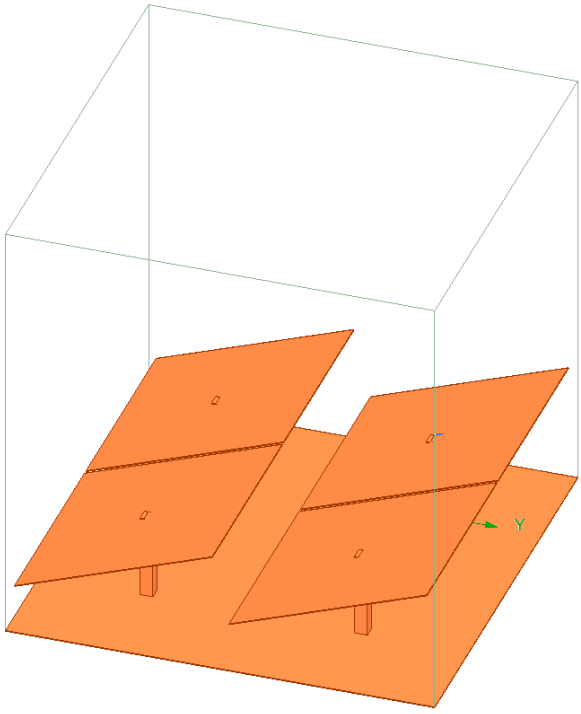

Figure 3.8: Two-by-two metasurface with tilted patches of 20 *degrees*.

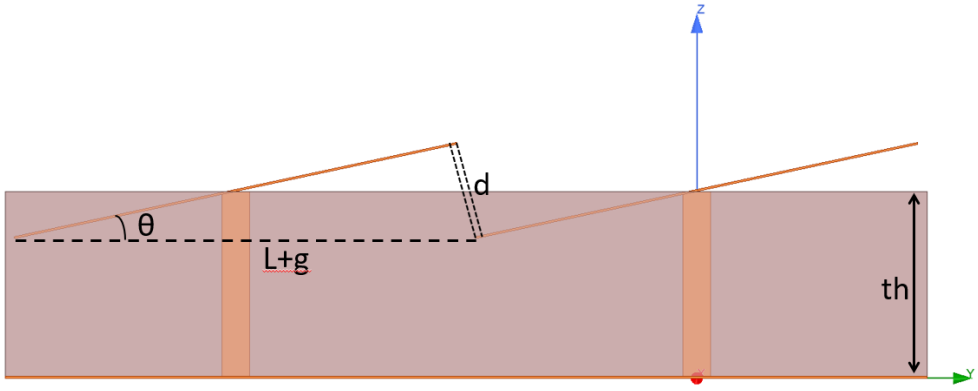

Figure 3.9: Overlap of patches from a two-by-two metasurface.

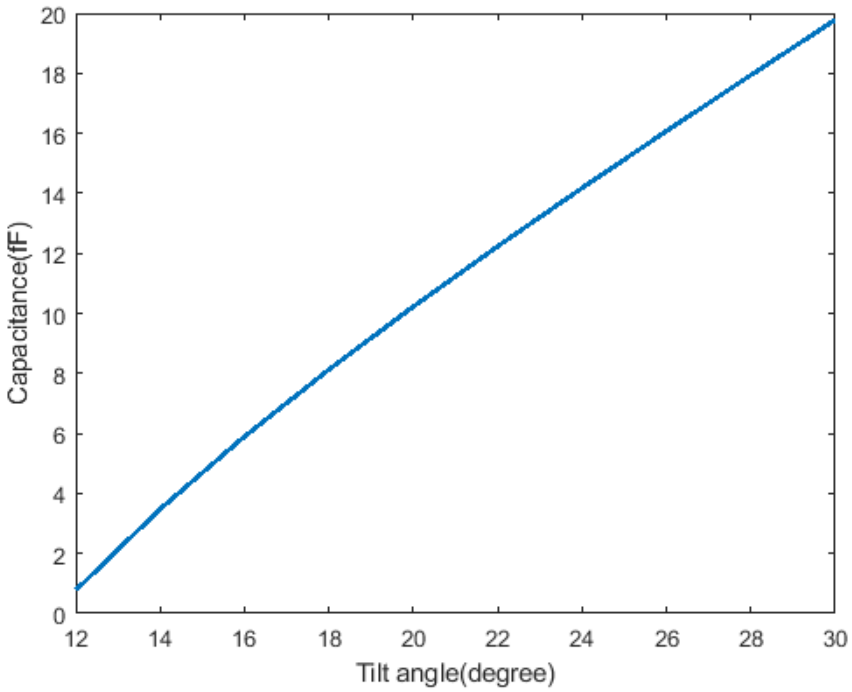

Figure 3.10: Capacitance of overlap area when tilt angle changes.

By running a parametric sweep in Ansys HFSS 2020R2, the tilt angle of the top patches changes from 12 *degrees* to 30 *degrees*. The magnitude and phase of reflection coefficient as a function of tilt angle and frequency are shown in Figure 3.11.

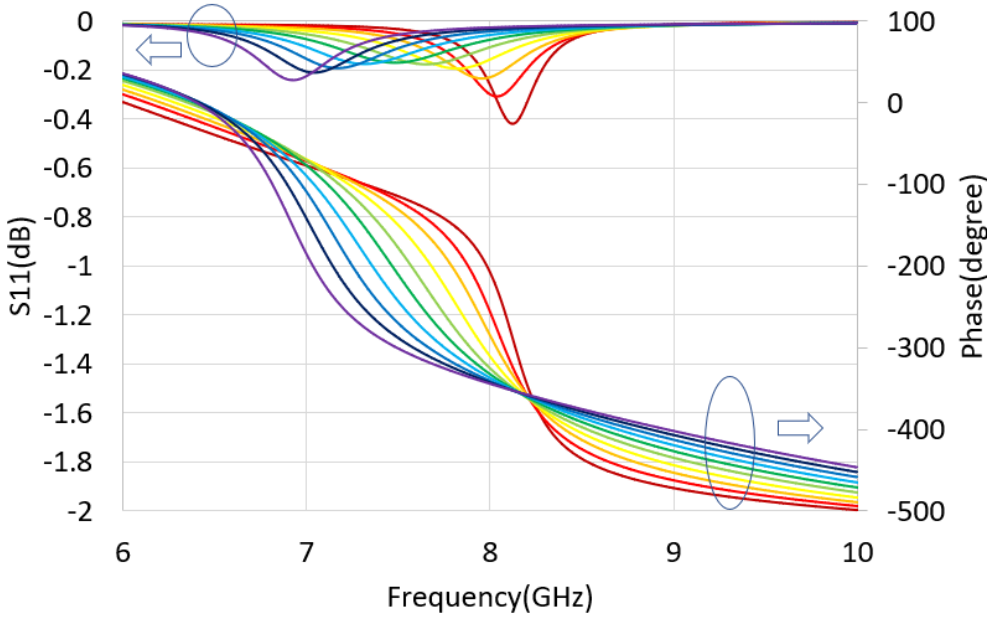

Figure 3.11: Magnitude and phase of reflection coefficient of a metasurface with tilted patches. From left to right: 30 *degrees*, 28 *degrees*, 26 *degrees*, 24 *degrees*, 22 *degrees*, 20 *degrees*, 18 *degrees*, 16 *degrees*, 14 *degrees*, and 12 *degrees*.

As the tilt angle increases, the capacitance of the overlap area increases, which leads to a lower resonance frequency. The phase tuning range at 7.5 GHz is around 180 *degrees*, which is much smaller than that required in the phase distribution calculated in section 3.1. This is caused by the relatively small quality factor of resonance, which may be solved by optimizing the structure's dimensions.

3.3 Tunable reflectarray

The mechanism of tunable metasurfaces focuses on adjusting the electrical characteristics between adjacent elements, whereas the mechanism underlying tunable reflectarrays focuses on tuning array units. Reflectarrays are more like a phased array without active feeds. Two types of tunable reflectarrays are discussed in this section.

3.3.1 Electrically tunable reflectarray

The first type is an electrically tunable reflectarray, which uses a varactor to change the capacitance. The reflection phase is thus also changed.

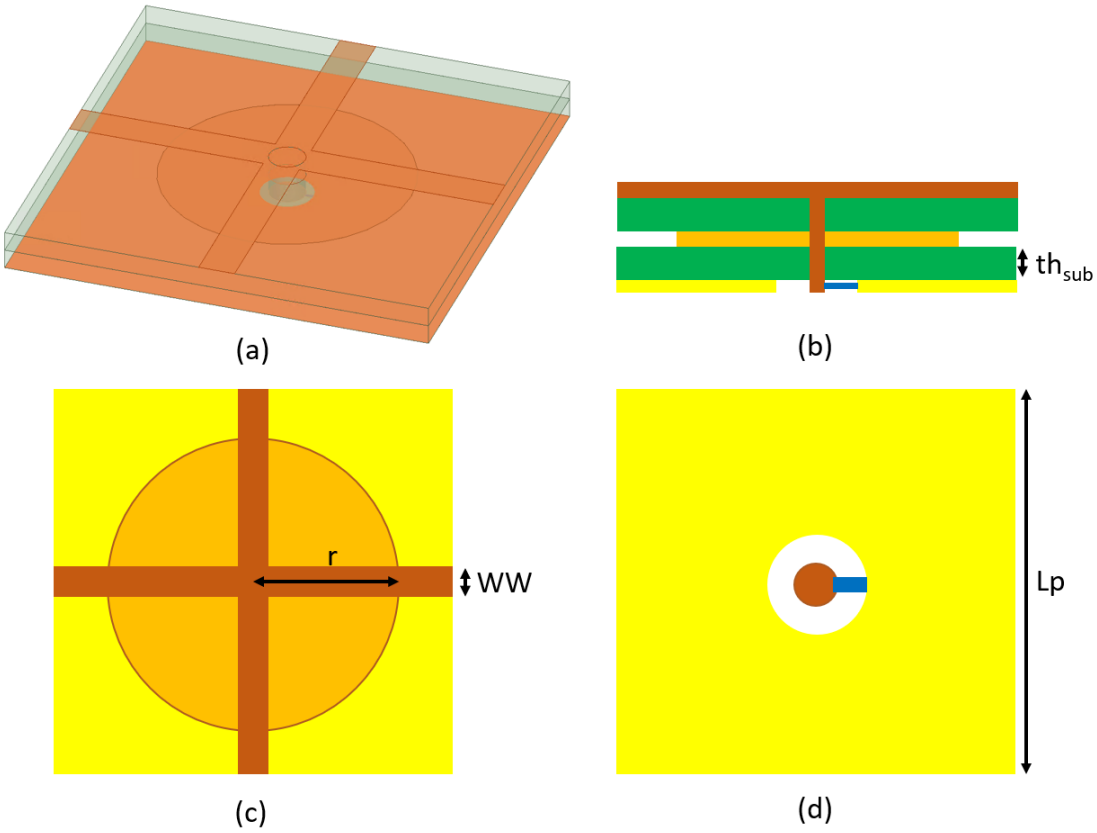

Figure 3.12: Unit cell of a tunable reflectarray with a varactor: (a) Trimetric view, (b) cross-section schematic, (c) top view schematic, and (d) bottom view schematic.

Each element of this design is made of three-layer PCB material, as shown in Figure 3.12. The brown, orange, and yellow blocks are conductor layers. Crosslines lay on the top layer and connect with a circular plate in the middle layer through a via hole. The bottom layer is a whole plane, except the via hole is isolated from that layer and a varactor is inserted in between. The green block in Figure 3.12 is a dielectric layer RO4350, with a dielectric constant of 3.66. The blue block represents a varactor that is used to change the reflection phase.

After a group of simulations and optimizations, a tunable reflectarray operating at 3.55 GHz is presented. The dimensions of the structure are listed in Table 3.1.

Table 3.1: Dimensions of a 3.55 GHz Tunable Reflectarray

Parameter	Value(mm)	Description
Lp	26	Length of crossline
r	12	Radius of middle plate
WW	2.2	Width of crossline
th_{sub}	0.762	Thickness of dielectric layer

By running a parametric sweep, with periodic boundary conditions set up in Ansys HFSS 2020R2, the capacitance of the varactor changes from 0.8 pF to 2.6 pF. The magnitude and phase of reflection coefficient versus frequency while changing capacitance are plotted in Figure 3.13.

As expected, the resonance frequency decreases from 3.64 GHz to 3.45 GHz as the capacitance of the varactor increases from 0.8 pF to 2.6 pF. The phase shift range is around 312 *degrees* at 3.55 GHz.

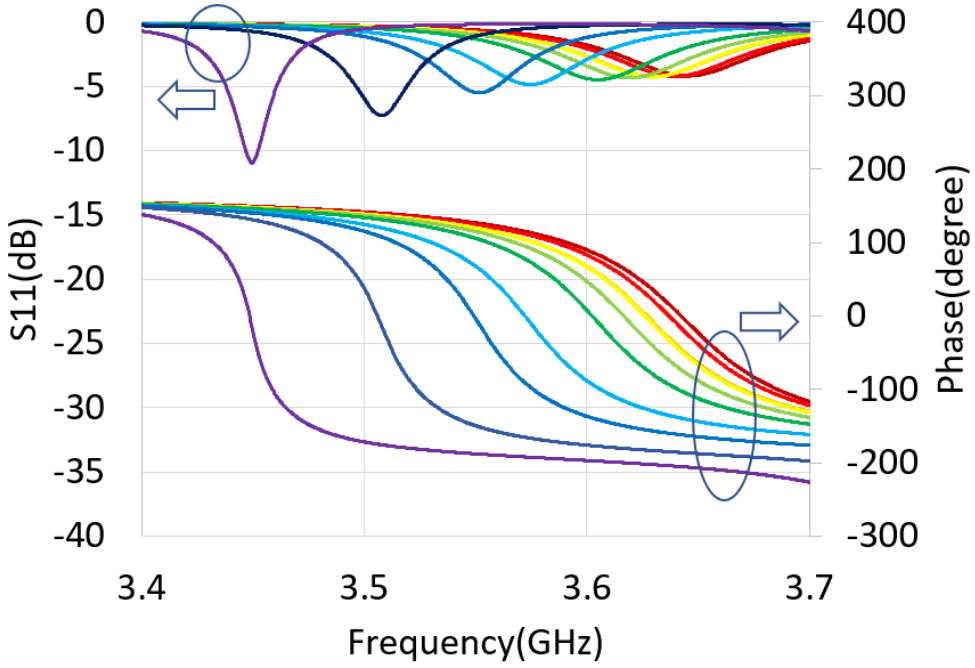

Figure 3.13: Magnitude and phase of reflection coefficient of a reflectarray with varactors. From left to right: 2.6 pF, 2.4 pF, 2.2 pF, 2 pF, 1.8 pF, 1.6 pF, 1.4 pF, 1.2 pF, 1 pF, and 0.8 pF.

3.3.2 Mechanically tunable reflectarray

The second type is a mechanically tunable reflectarray that is able to change the reflection phase by the mechanical movement of the middle plate.

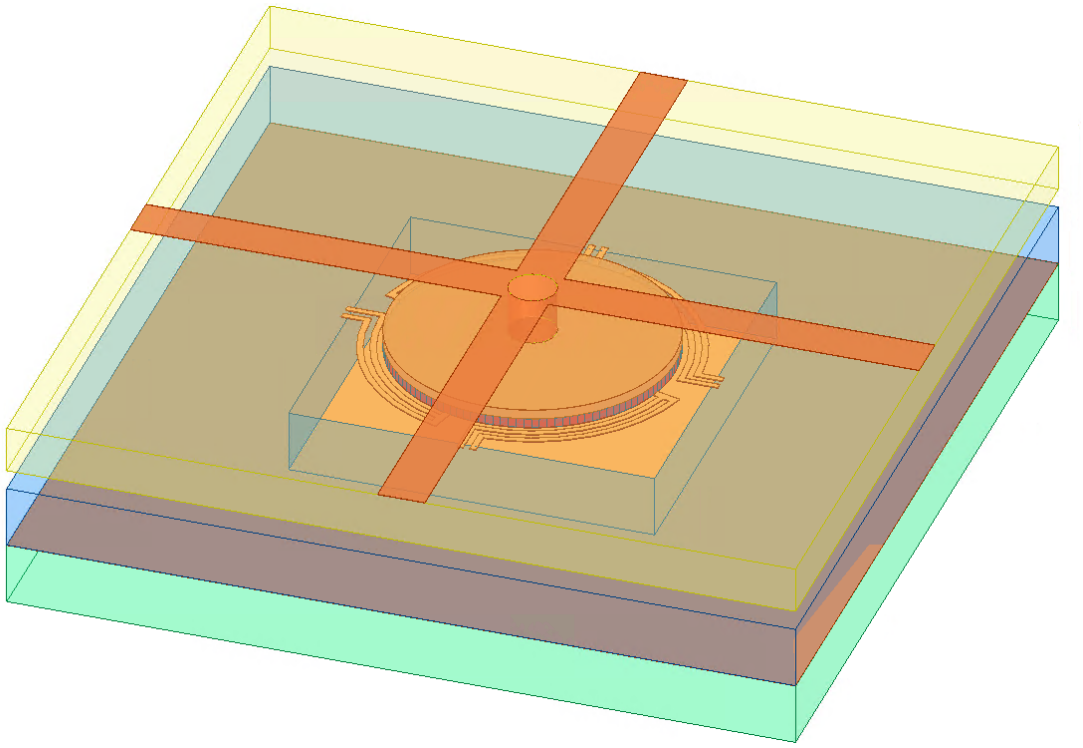

Figure 3.14: Unit cell of a mechanically tunable reflectarray.

It can be seen from the cross-section schematic in Figure 3.15 that this structure consists of three layers. The structure of layer1 is similar to the top layer and the middle layer combined in the electrically tunable reflectarray shown in section 3.3.1. They all have cross lines on top, connected with a circular plate through a via hole. However, the material of the dielectric substrate in layer1 is alumina. Layer2 is a MEMS structure for the mechanical movement of the middle plate. The plate at the central part is made of gold, silicon, and silicon dioxide. This plate is supported by four bimorph beams used to achieve movement. Layer3 is made of a gold plane on a PCB substrate.

This reflectarray can be modeled as layer1 connected with an equivalent capacitor in series, as shown in Figure 3.16. It's formed between the bottom patch of layer1 and the

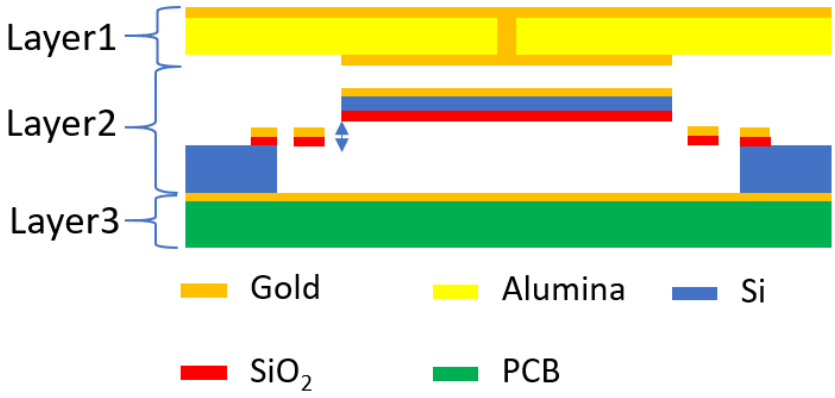

Figure 3.15: Cross-section of a mechanically tunable reflectarray.

top patch of layer2. The capacitance can be changed by the mechanical movement of the central plate, which leads to a resonance frequency shift and a reflection phase change.

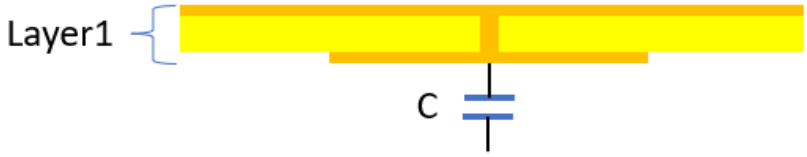

Figure 3.16: Equivalent circuit model of mechanically tunable reflectarray.

Simulations are done in Ansys HFSS 2020R2 by a parametric sweep with periodic boundary conditions. The central plate is moved up from 0 um to 20 um. The corresponding magnitude and phase of reflection coefficient are plotted in Figure 3.17.

The simulation results show that as the central plate moves up from 0 um to 20 um, the resonance frequency decreases from 54.9 GHz to 54.2 GHz. The phase shift achieved at 54.5 GHz is around 237 $degrees$.

In conclusion, Four different metasurfaces and reflectarrays are brought and the phase tuning range achieved are listed in Table 3.2.

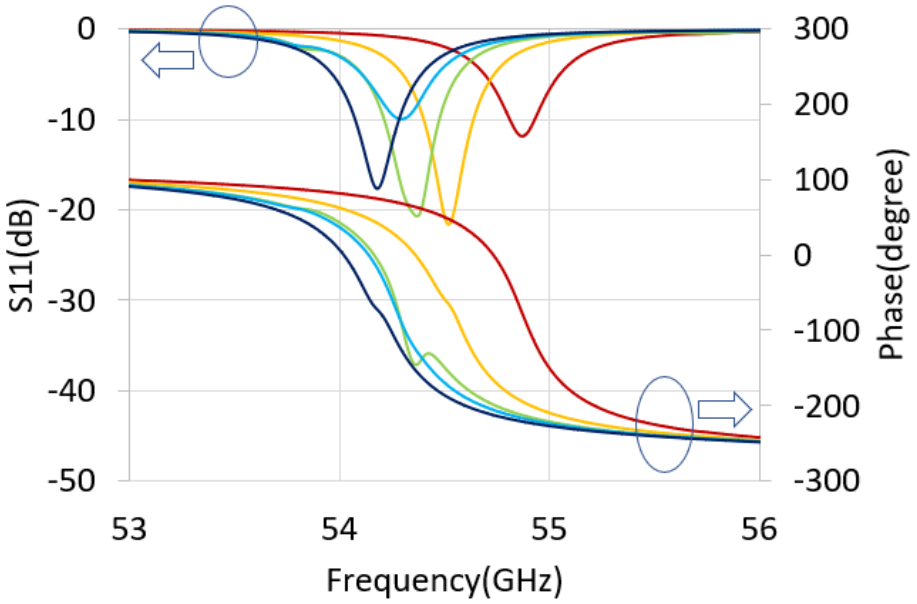

Figure 3.17: Magnitude and phase of reflection coefficient of a mechanically tunable reflectarray. From left to right: 20 um, 15 um, 10 um, 5 um, and 0 um.

Table 3.2: Phase Tuning Range of Four Tunable Designs

	Electrical tuning	Mechanical tuning
Metasurface	360° @ 4 GHz	180° @ 7.5 GHz
Reflectarray	312° @ 3.55 GHz	237° @ 54.5 GHz

Chapter 4

Fabrication and Measurement

One of the typical methods for measuring reflectarrays is placing a prototype at the open end of a transverse-electric rectangular waveguide. However, a waveguide has specific dimensions corresponding to its operating frequency range, which limits the size of the arrays to be tested. For example, a WR284 rectangular waveguide works at frequencies from 2.6 GHz to 3.95 GHz with dimensions of 72.136 $mm \times 34.036$ mm. The dimensions of an individual unit on the proposed electrically tunable reflectarray are 26 $mm \times 26$ mm, which means only three units in a row can be tested using such a rectangular waveguide. This is insufficient to imitate the periodic boundary condition.

In the present chapter, a practical design and experimental setup of the electrically tunable reflectarray mentioned in section 3.3.1 is introduced.

4.1 Circuit design and chip selection

The proposed electrically tunable reflectarray is made of a three-layer PCB with varactor chips embedded on the bottom layer. Of the various varactor chips available, SMV1405, a plastic-packaged abrupt junction tuning varactor from SKYWORKS, is chosen because of its capacitance tuning range (0.8 pF to 4.1 pF), operating frequency (up to 10 GHz), and relatively high quality factor (3200 at 4 V, 50 MHz). A biasing network is designed to control the varactor diode. The schematic circuit was simulated in Advanced Design System (ADS) 2019, as shown in Figure 4.1.

The circuit made of components inside the red dash line is the SPICE model of the varactor diode from the datasheet of SMV1405. The varactor is reversely biased, with a

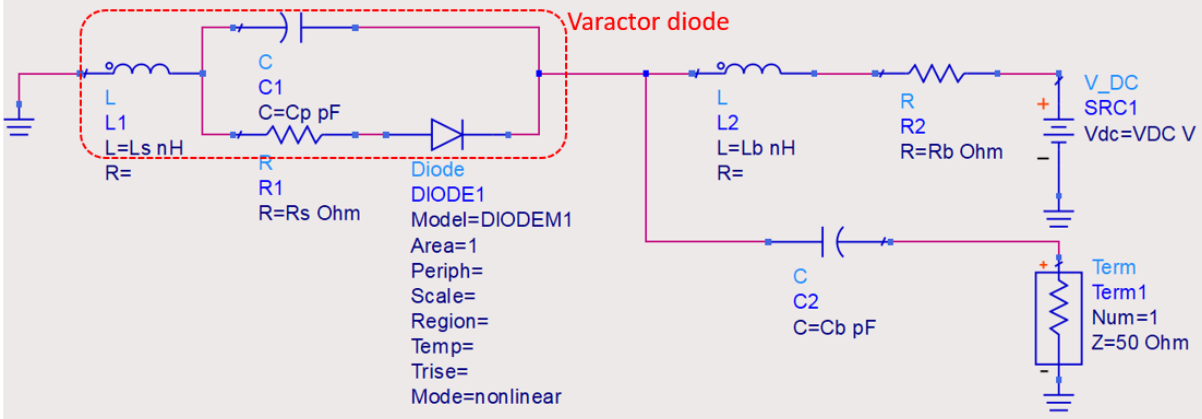

Figure 4.1: Schematic of biasing network for a varactor diode.

DC voltage connected through a resistor and an inductor. An RF signal is fed into the cathode of the varactor through a large value capacitor, which is used to block RF signals from the DC voltage input.

Initially, the resistor value is determined to be 1 $M\Omega$, because the varactor is reversely biased. This means the current is limited to a maximum of 20 nA when the maximum DC voltage is 20 V. Considering the need for heat dissipation and space limitation of the reflectarray, a surface-mounted resistor chip with a 0603 package footprint is picked.

The choices of inductor and capacitor need to ensure that their self-resonance frequency is away from the operating frequency, which is 3.5 GHz in this design.

There are many available options for surface mount inductor chips. LQP03HQ4N7H02D from Murata Electronics, with a value of 4.7 nH, is chosen as the initial inductor because it has a quality factor of 20 and a self-resonance frequency of 7.0 GHz to 9.5 GHz. In this case, the resonance of the inductor and the varactor diode is between 1.1 GHz and 2.6 GHz according to $f = \frac{1}{2\pi\sqrt{LC}}$, which is far away from the operating frequency of 3.5 GHz.

The capacitance of the fixed capacitor should be relatively large, as it is connected in series with the varactor diode. A simulation is done at 3.5 GHz with $C2 = 5\,pF,\ 10\,pF,\ 100\,pF$ to find the best capacitance value for the fixed capacitor, as plotted in Figure 4.2. The capacitance values are calculated based on the Z parameters of the simulation results using the equation:

$$C = -\frac{1}{2\pi f \times im(z11) \times 10^{12}}. \tag{4.1}$$

As can be seen in the figure, when the fixed capacitor is 10 pF or 100 pF, the equivalent

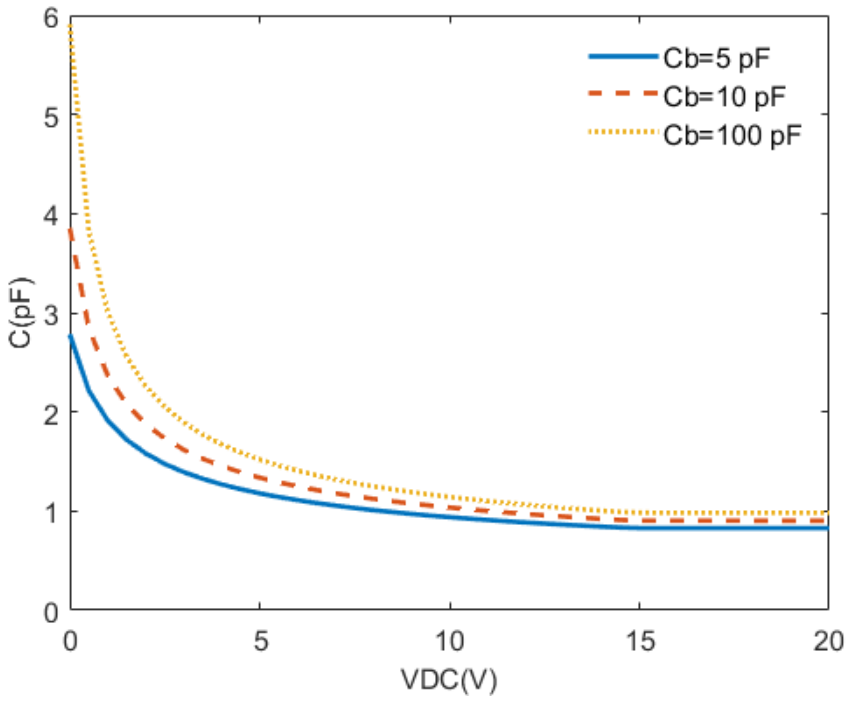

Figure 4.2: Equivalent capacitance simulated using a fixed capacitor with different values.

capacitance tuning range of the whole circuit is sufficiently wide to achieve the performance of the varactor diode claimed in its datasheet. Larger capacitance, however, means smaller quality factor and lower self-resonance frequency, according to Figure 4.3 from the datasheet of the capacitor chips [83]. With a capacitance at 10 pF, the quality factor is relatively high and the self-resonance frequency is around 4 GHz, which is slightly higher than the operating frequency of 3.5 GHz.

All the chips selected in the circuit are listed in Table 4.1. A simulation in the frequency range 3 GHz to 4 GHz is done and the equivalent capacitance is plotted in Figure 4.4, which shows that while the capacitance is not constant within the frequency range of 3 GHz to 4 GHz, it does not change much when 1 V DC voltage or more is applied.

Table 4.1: Final Chip Selection

Ref.	Type	Value	Package	Part NO.
-	Varactor	-	0402	SMV1405-040LF
R2	Resistor	1 $M\Omega$	0603	CRGP0603F1M0
L2	Inductor	4.7 nH	0201	LQP03HQ4N7H02D
C2	Capacitor	10 pF	0603	600S100GW250XT

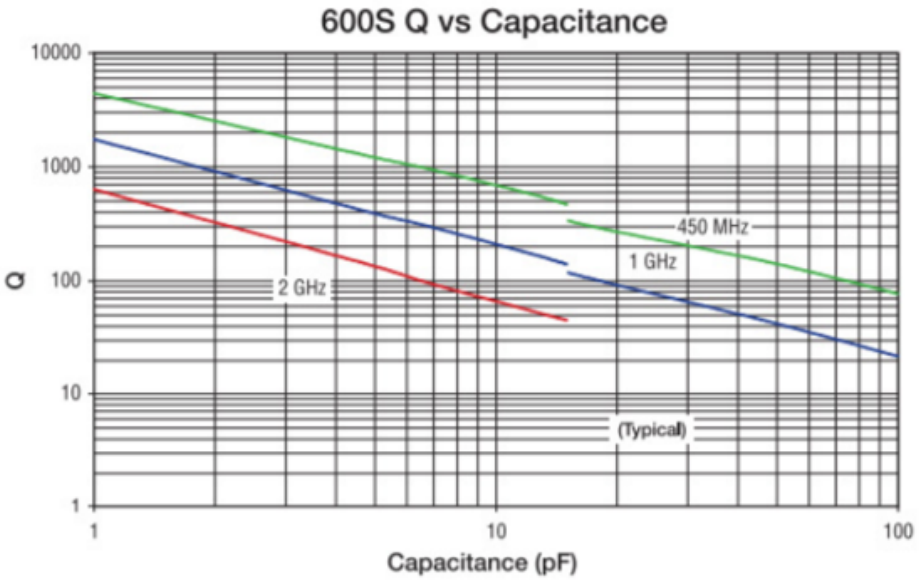

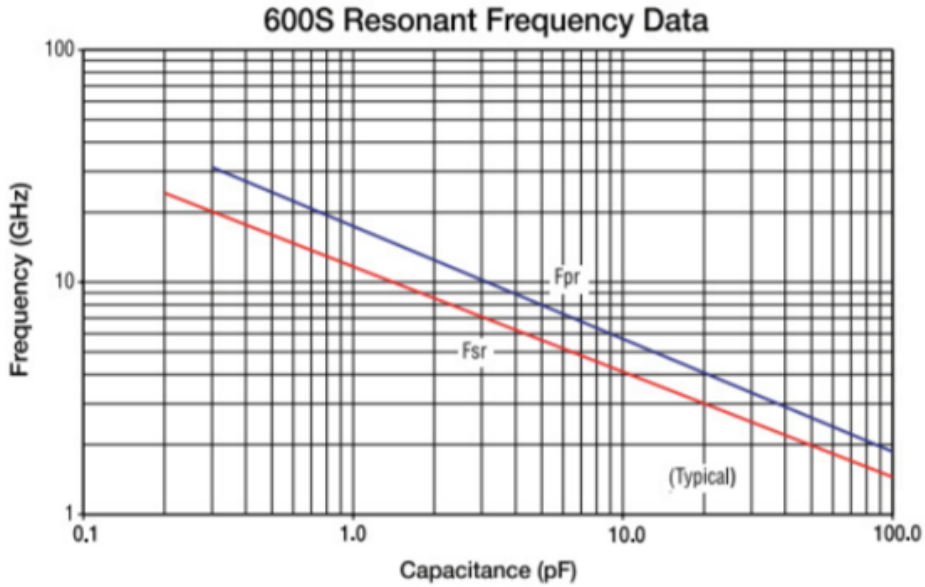

Figure 4.3: Quality factor vs capacitance and self-resonance frequency vs capacitance of surface mount capacitor 600S series from American Technical Ceramics [71].

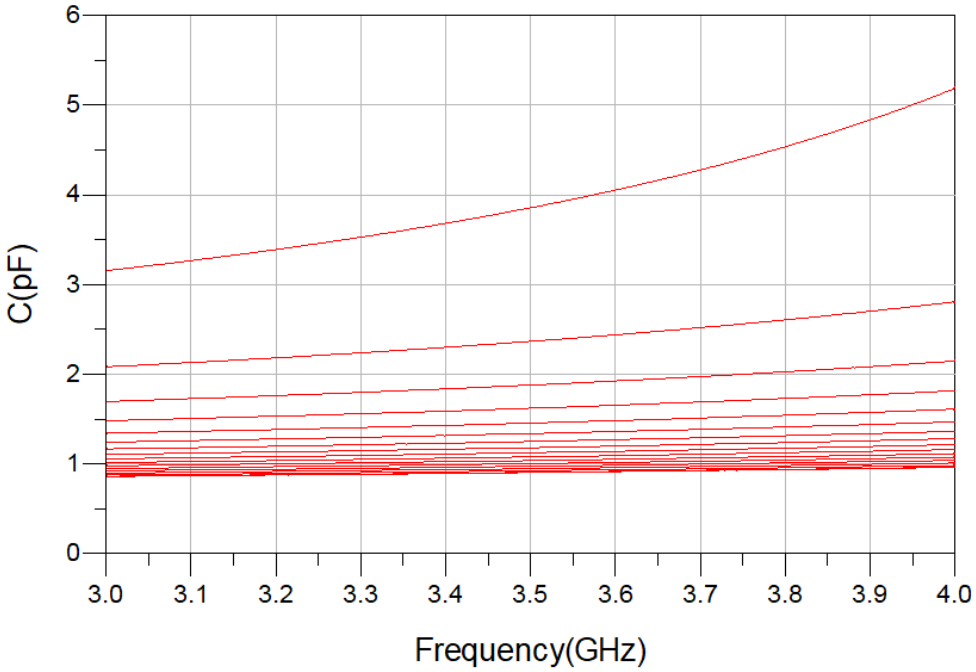

Figure 4.4: Equivalent capacitance vs frequency when different DC voltage are applied (0 V to 20 V from the top trace to the bottom trace with an increment of 1 V).

4.2 PCB layout

The next step toward fabrication is creating a PCB layout based on the circuit schematic and parts package footprints. A 3D view of the layout in a three-layer structure is plotted in Figure 4.5, with the distance between each layer enlarged 10 times the actual distance.

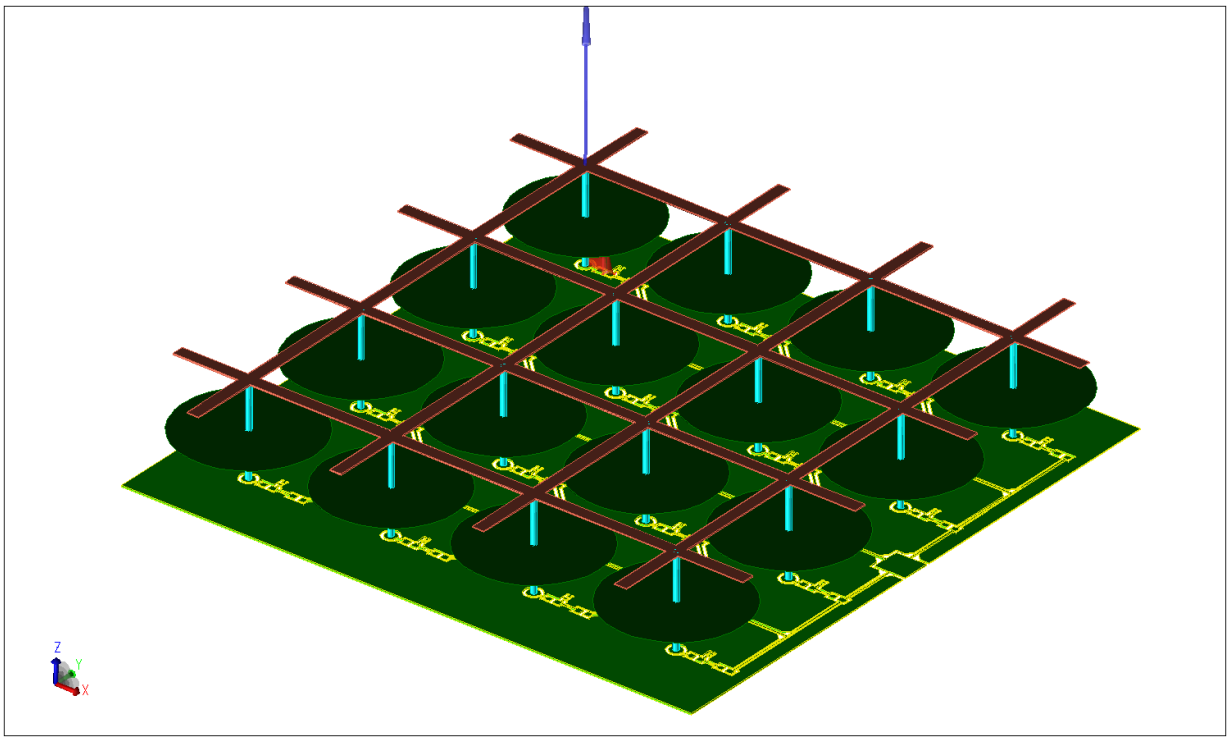

Figure 4.5: Layout of electrically tunable reflectarray in 3D view.

This board consists of 16 identical units connected through cross lines on the top layer. There are also 16 metal discs in the middle layer that are used to form a fixed capacitor between that layer and the bottom one. All the varactor diodes are fed with the same DC voltage to achieve the same capacitance. The routing of the DC voltage supply is plotted in Figure 4.6. Details of the biasing network for each varactor diode are shown in Figure 4.7.

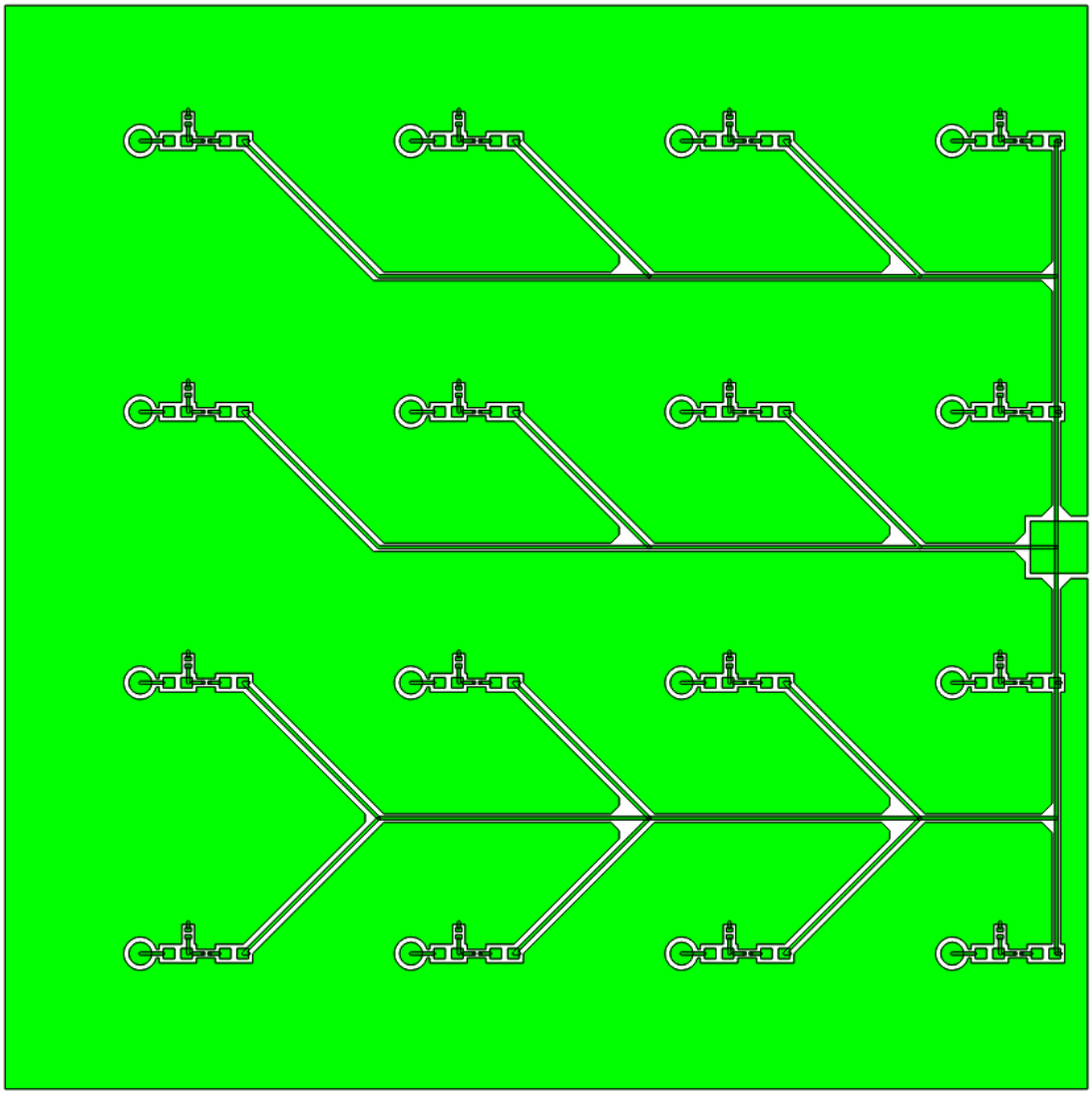

Figure 4.6: Layout of bottom layer of electrically tunable reflectarray.

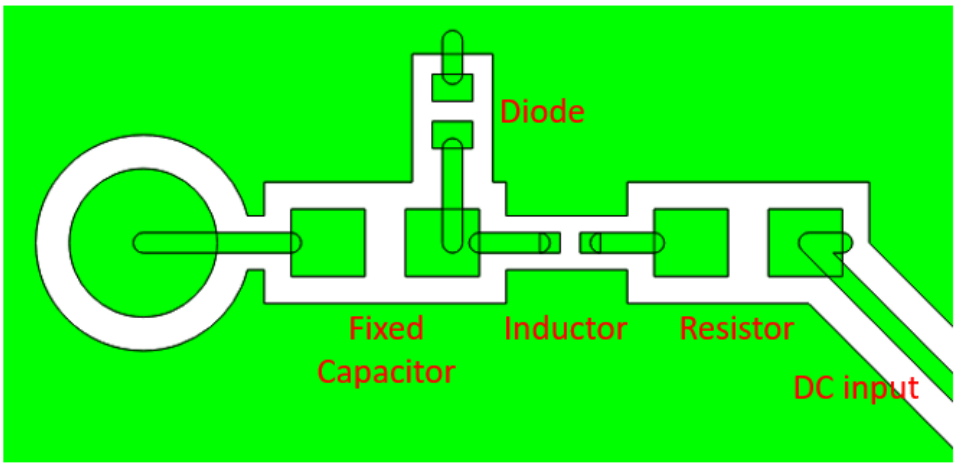

Figure 4.7: layout of the biasing network for a varactor diode.

4.3 Measurement

4.3.1 Reflectarray measurement

The proposed reflectarray was fabricated and assembled according to the layout designed as shown in Figure 4.8.

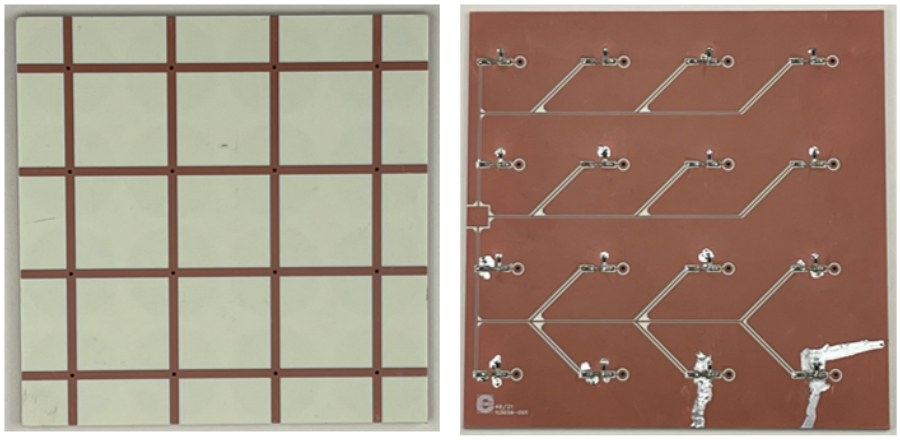

Figure 4.8: Top view and bottom view of the proposed reflectarray board.

To investigate the performance of the reflectarray board with four-by-four unit cells, a vertically illuminated plane wave directly incidents on top of the board; the reflected wave can then be measured to calculate the board's performance. As mentioned earlier, a normal waveguide was proven unsuitable for this measurement, because the waveguide cross-section is too small compared with the board size. A horn antenna, on the other hand, is useful, as it can provide a significant level of directivity and gain and a plane wave at the horn's edge, as shown in Figure 4.9.

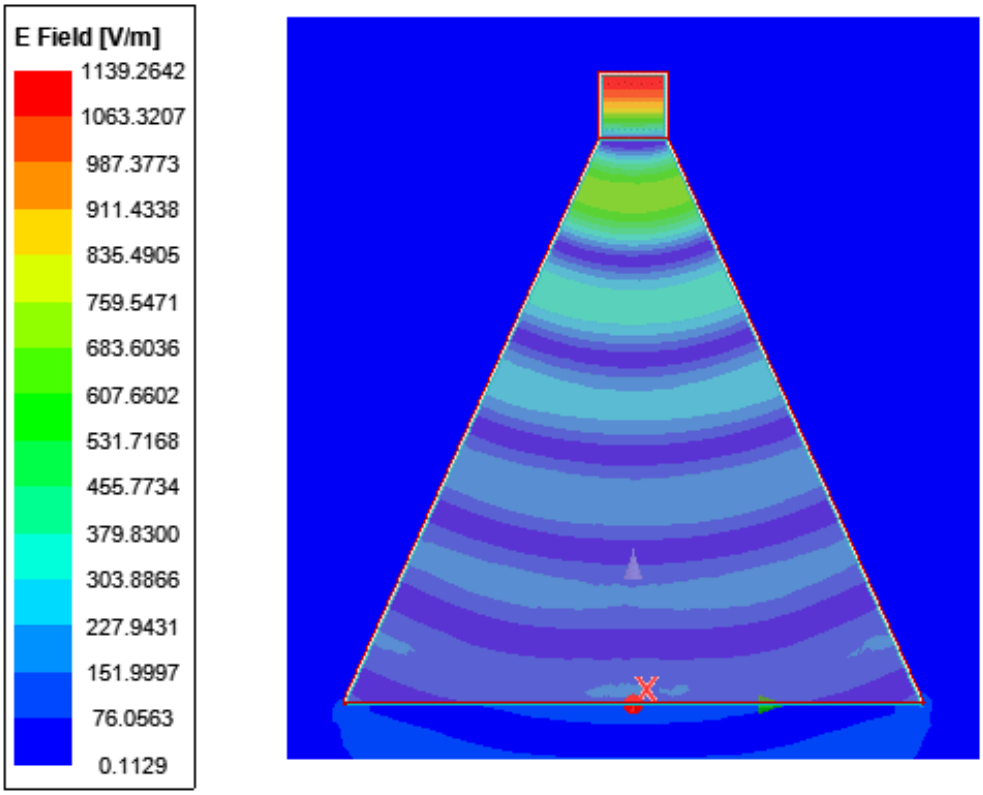

Figure 4.9: Electric field distribution in a horn antenna.

A WR-284 waveguide horn antenna operating from 2.6 GHz to 3.95 GHz was tested in a lab environment to determine the influence of background noise and signal reflections. When the power of the source from the network analyzer was set to 0 dBm, S_{11} was measured from the horn antenna, as plotted in Figure 4.10. It can be clearly seen in the figure that when there is nothing attached to the horn antenna, S_{11} between 3.3 GHz and 3.7 GHz is in the range of -36 dB to -17 dB.

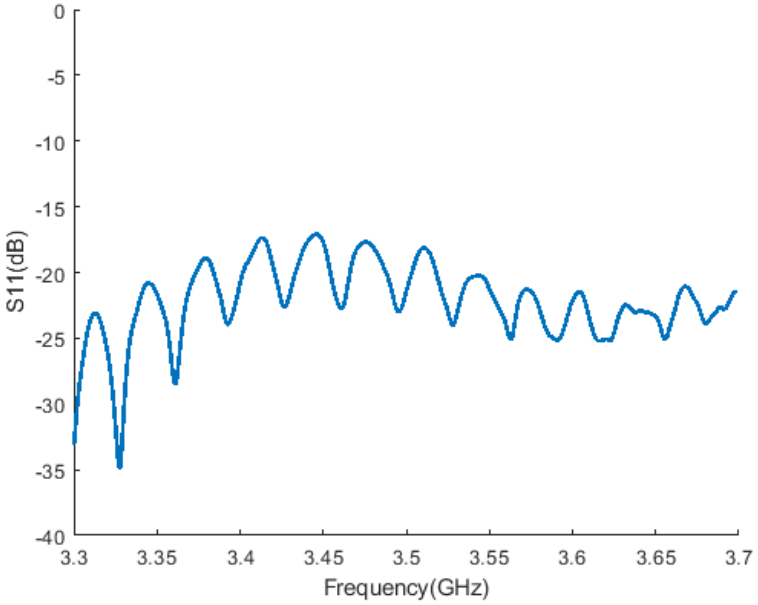

Figure 4.10: S_{11} of a WR-284 horn antenna tested in a lab environment.

The reflectarray board was then bonded at the edge of the horn antenna using taps, as shown in Figure 4.11. The reflection coefficient in this situation was measured using a network analyzer and plotted in Figure 4.12. There was no resonance at the expected operating frequency of 3.5 GHz.

To minimize the interference from the background noise, the reflectarray was placed inside the horn antenna, which was closer to the feed port. The reflection coefficient was measured three times when the DC voltage to the varactor diodes was set to 0 V, 10 V and 20 V, as shown in Figure 4.13. There is resonance around it, 3.5 GHz but the curves barely changed when the DC voltage was varied.

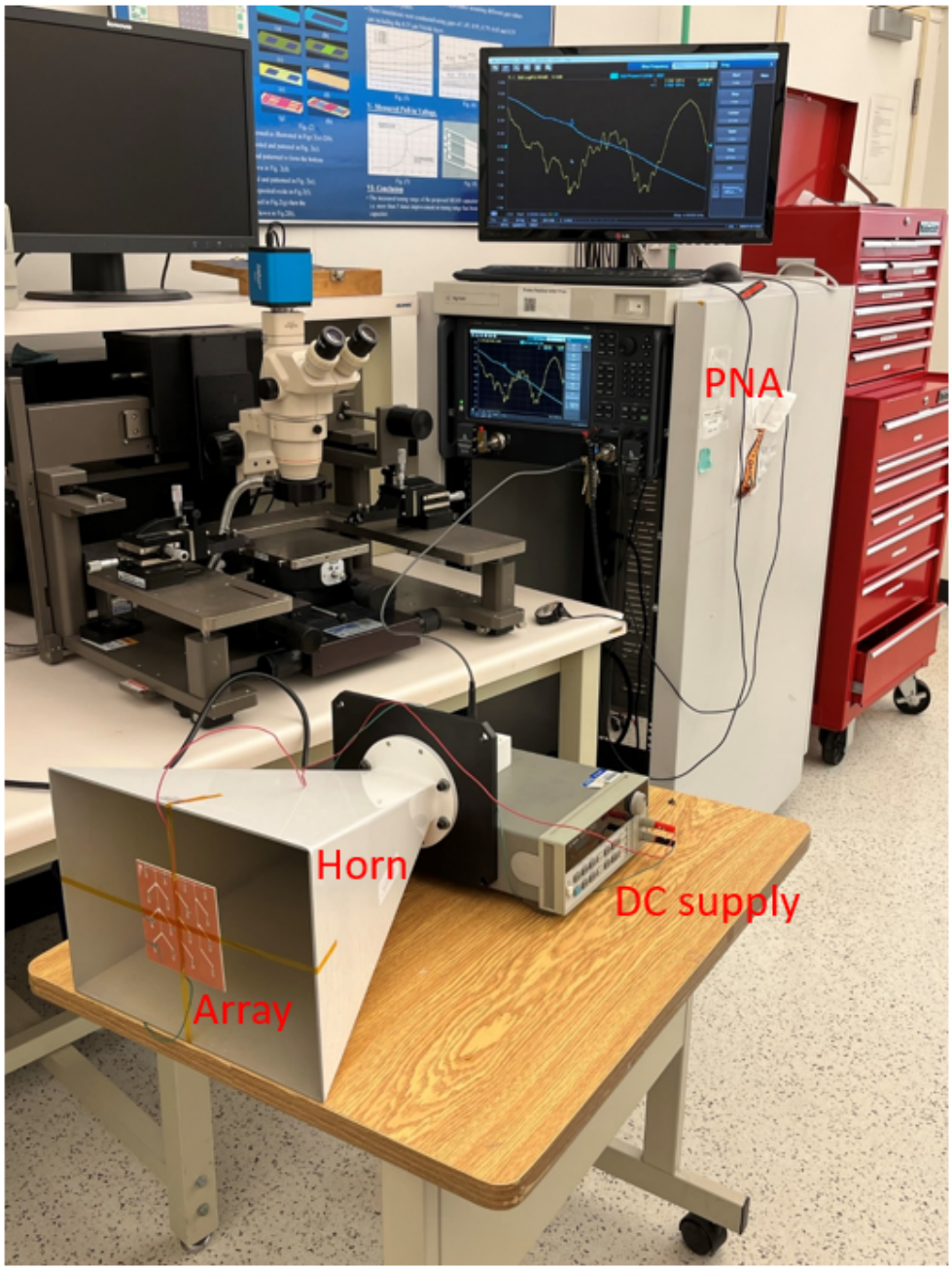

Figure 4.11: Test setup, including a reflectarray board, a WR-284 horn antenna, DC voltage, and a network analyzer.

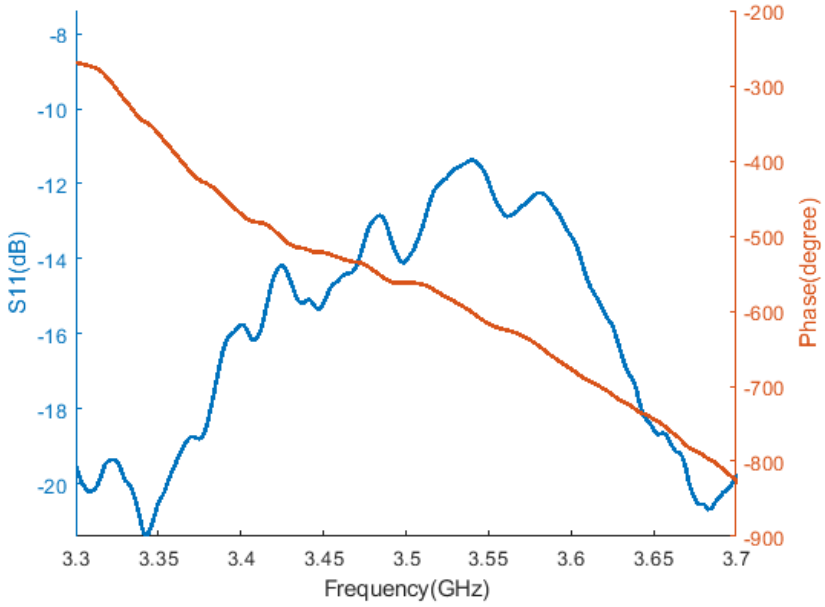

Figure 4.12: S_{11} of the horn antenna with a reflectarray attached at the open end.

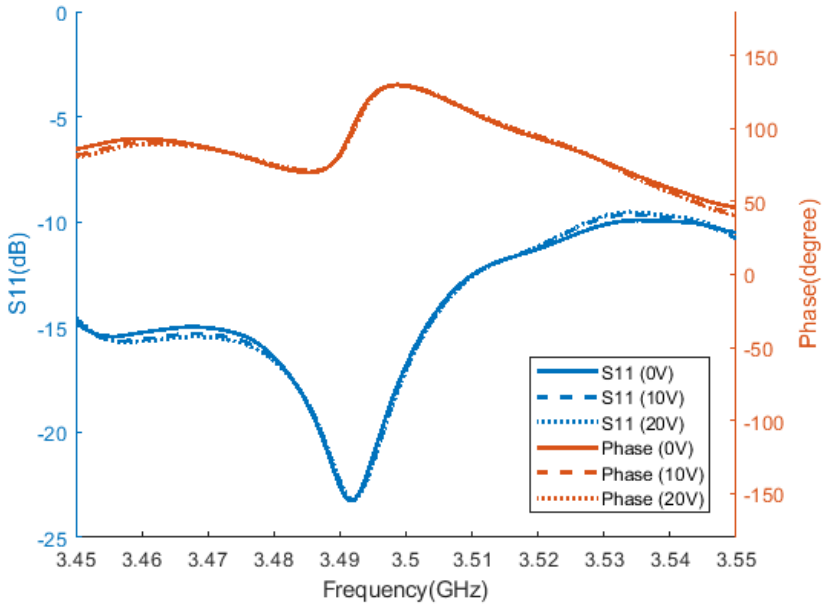

Figure 4.13: S_{11} of the horn antenna when a reflectarray was placed inside the horn.

4.3.2 Varactor diode measurement

To investigate the reason for the lack of tunability, the varactor diode SMV1405 was tested on another board, as shown in Figure 4.14. The board is made of FR4 with a thickness of 1.6 mm. The input signal was fed to the circuit through a transmission line that was reduced to the point where it could barely hold the pins of the SMA connector, as shown in Figure 4.14. The DC voltage was connected with the varactor cathode to vary the capacitance.

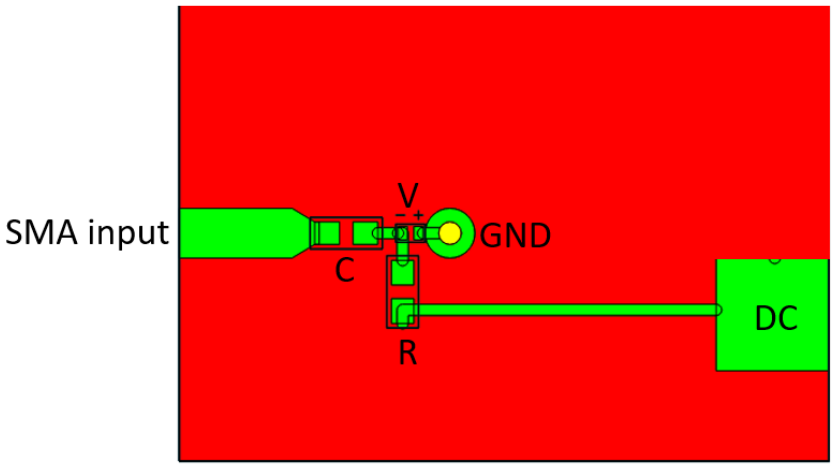

Figure 4.14: Layout of the board for varactor testing.

The capacitance of the circuit could be calculated based on the Z parameters that were measured using the network analyzer from Equation 4.2:

$$C = -\frac{1}{2\pi f \times imag(Z_{11})} \tag{4.2}$$

The quality factor could be calculated using Equation 4.3:

$$Q = abs[\frac{imag(Z_{11})}{real(Z_{11})}] \tag{4.3}$$

The simulation and measurement results of the capacitance and quality factor of the case where a short transmission line is used are plotted in Figure 4.15.

It can be clearly seen that the capacitance changes as the DC voltage varies. The measurement capacitance tuning range is 0.42 pF to 1.33 pF at 3.5 GHz. This is much

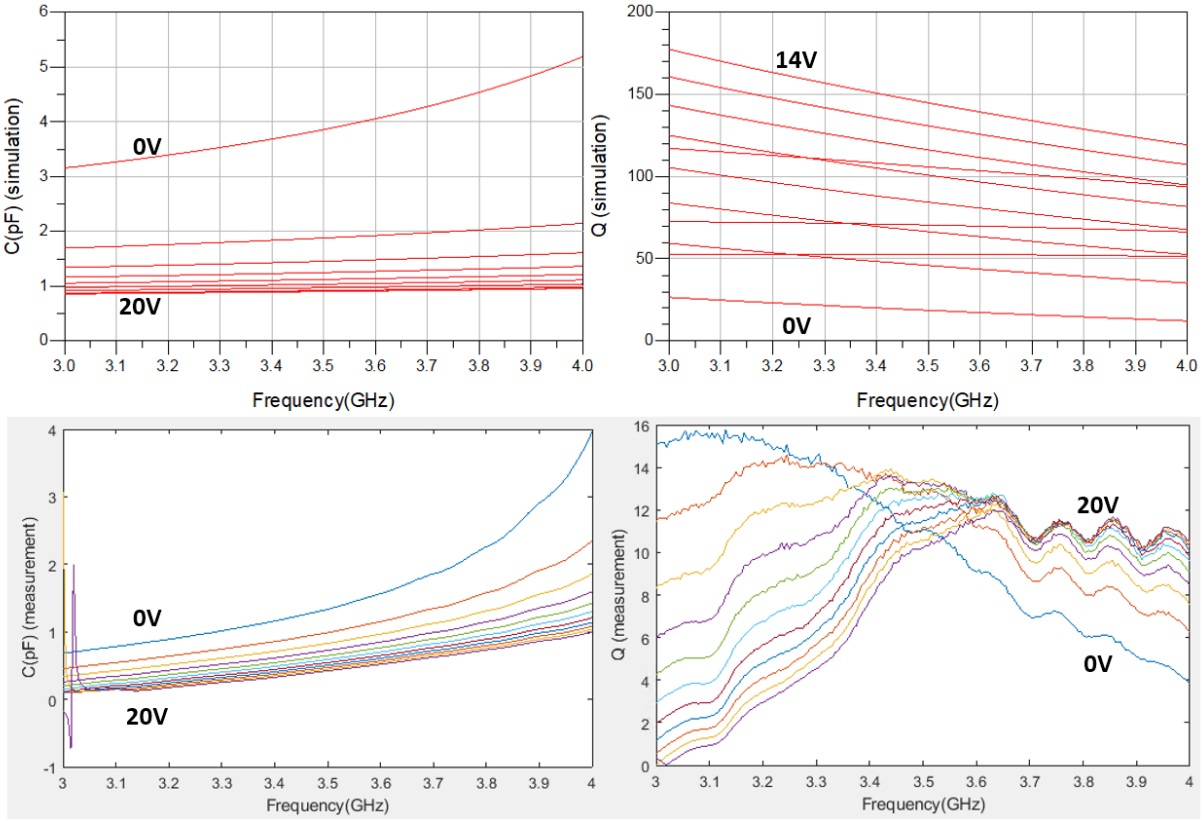

Figure 4.15: Upper: Simulation results of capacitance and Q. Lower: Measurement results of capacitance and Q.

smaller than the simulation capacitance tuning range, which is 0.92 pF to 3.86 pF at 3.5 GHz. The measured quality factor is also smaller than the simulation results.

The transmission line is designed for 3.5 GHz, whereas the capacitance and Q factor are useful only at 3.5 GHz.

4.3.3 Reflectarray measurement without varactor chips

To verify the performance of the board itself, a bare board of the proposed reflectarray without any varactor chips was tested under the same experimental setup using a horn antenna and network analyzer. It was confirmed that influence from the background was similar to the previous test and kept under -17 dB in the range of 3 GHz to 4 GHz, as shown in Figure 4.16.

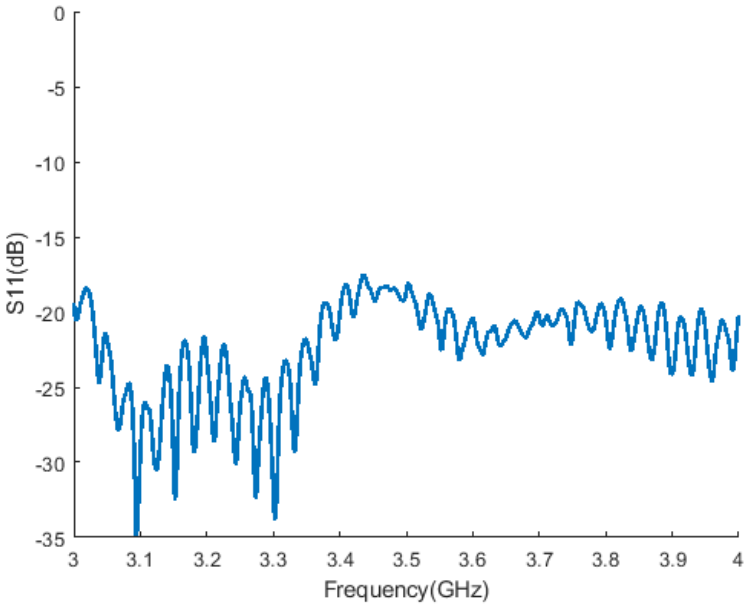

Figure 4.16: S_{11} of a WR-284 horn antenna tested in a lab environment.

The bare board was then placed at the edge of the horn antenna and inside the horn antenna, as shown in Figure 4.17.

Both the measurement and simulation results in these arrangements are plotted in Figure 4.18. Similar resonances occurred at around 3.6 GHz except when the array was place

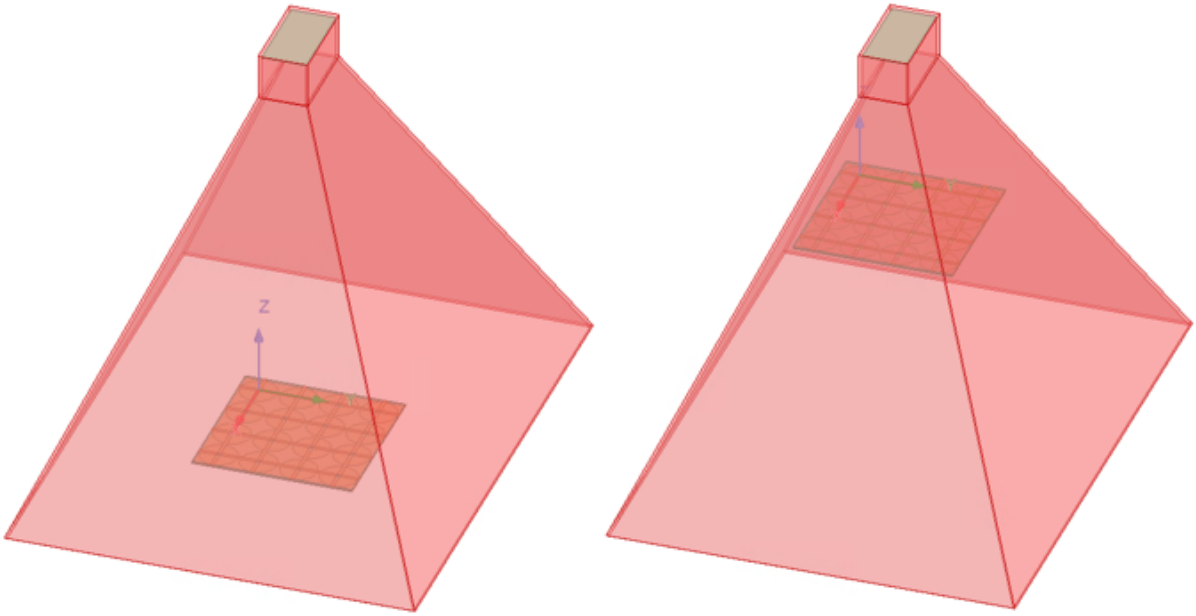

Figure 4.17: Left: Simulated structure when the array was placed at the edge of horn antenna. Right: Simulated structure when the array was placed inside the horn antenna.

at the edge of horn antenna, the resonances were highly influenced by the background noise and reflection noise. When the board was placed inside the horn antenna, the results plots in measurement and simulation shared similar characteristics including slightly different resonance frequencies, and similar phase shift curves. The above results show that the board without chips had a resonance frequency as designed but due to the limitation of experimental setup, the performance was not tested accurately.

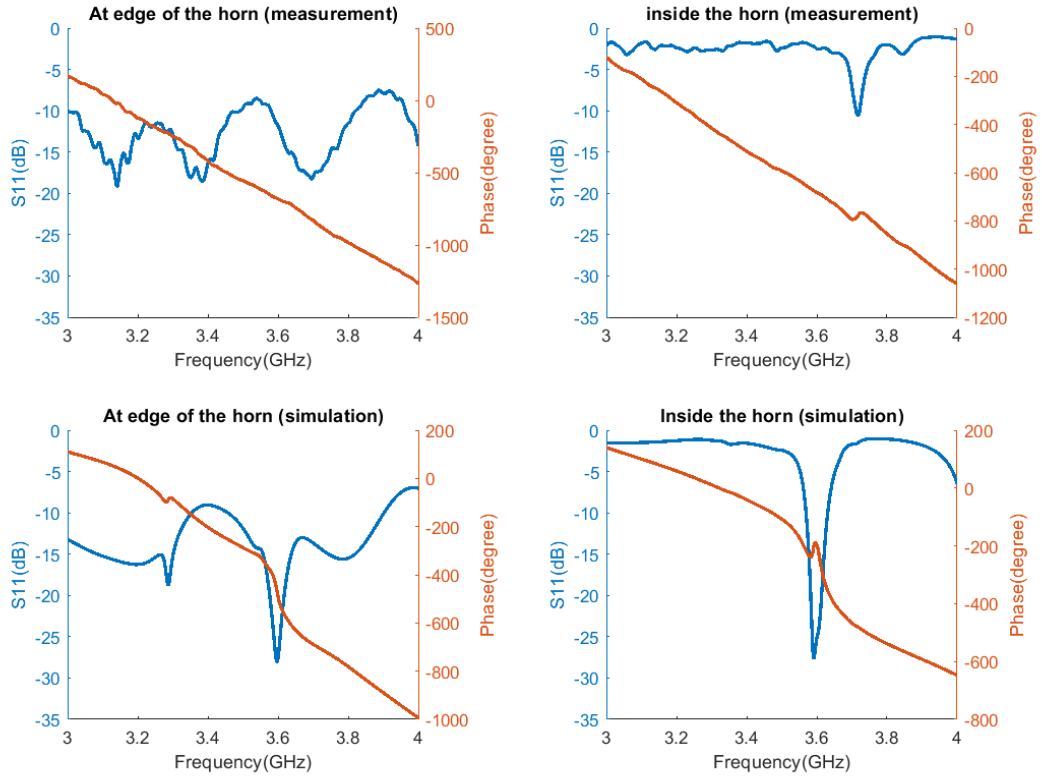

Figure 4.18: Left: Measurement and simulation S_{11} results when the array was placed at the edge of the horn antenna. Right: Measurement and simulation S_{11} results when the array was placed inside the horn antenna.

Chapter 5

Conclusion

5.1 Summary of research

The main contributions of this thesis can be summarized as follows:

The design and performance investigation of several tunable metasurface and reflectarray models were conducted. Based on the simulation of the particular structures stated, the electrically tunable metasurface achieved a phase shift range of 360 degrees, the mechanically tunable metasurface achieved a phase shift range of 180 degrees, the electrically tunable reflectarray achieved a phase shift range of 312 degrees, and the mechanically tunable reflectarray achieved a phase shift range of 237 degrees.

The proposed electrically tunable reflectarray was realized using varactor diodes SMV1405. The circuit was designed to realize a four-by-four array consisting of identical units. A biasing network of varactors was carefully chosen to maximize the normalized quality factor.

Reflectarrays with and without varactors were measured using an S-band horn antenna. The measurement results show that the resonances occur at a frequency that is slightly different from that of the simulation results.

5.2 Future work

In the current experimental setup, the array was tested using a horn antenna in the lab, where background noise cannot be ignored. The array was placed either at the edge of

the horn or inside the horn, which led to non-planar incident waves. Performing the measurements in an anechoic chamber would be the optimal test setup.

The current design lacks tunability, which could be due to a low quality factor varactor diode. The mechanically tunable metasurface and reflectarray would not suffer from the varactors' limitations. The mechanical movement of array units could be better realized using actuators based on micro-electro-mechanical systems (MEMS) technology.

References

[1] D. Berry, R. Malech, and W. Kennedy, "The reflectarray antenna," *IEEE Transactions on Antennas and Propagation*, vol. 11, no. 6, pp. 645–651, 1963.

[2] C. S. Malagisi, "Microstrip disc element reflect array," *Electronics and Aerospace Systems Convention*, pp. 186–192, 1978.

[3] J. P. Montgomery, "A microstrip reflectarray antenna element," *Antenna Applications Symposium*, 1978.

[4] R. J. Mailloux, *Phased array antenna handbook*. Artech house, 2017.

[5] P. Nayeri, F. Yang, and A. Z. Elsherbeni, *Reflectarray antennas: theory, designs, and applications*. John Wiley & Sons, 2018.

[6] D. C. Chang and M. C. Huang, "Multiple polarization microstrip reflectarray antenna with high efficiency and low cross polarization," *IEEE Transactions on Antennas and Propagation*, vol. 43, no. 8, pp. 829–834, 1995.

[7] R. D. Javor, X. Wu, and K. Chang, "Design and performance of a microstrip reflectarray antenna," *IEEE Transactions on Antennas and Propagation*, vol. 43, no. 9, pp. 932–939, 1995.

[8] K. Chen, C. C. Tzuang, and J. Huang, "A higher order microstrip reflectarray at ka band," *IEEE Antennas and Propagation Society International Symposium Digest*, pp. 566–569, 2001.

[9] Y. Zhuang, J. Litva, F. Wu, and K.-L. Wu, "Modelling studies of microstrip reflectarrays," *Microwaves, Antennas and Propagation, IEE Proceedings* -, vol. 142, pp. 78 – 80, 03 1995.

[10] D. G. Gonzalez, G. E. Pollon, and J. F. Walker, "Microwave phasing structures for electromagnetically emulating refl ective surfaces and focusing elements of selected geometry," Feb 1990.

[11] S. Targonski and D. Pozar, "Analysis and design of a microstrip reflectarray using patches of variable size," in *Proceedings of IEEE Antennas and Propagation Society International Symposium and URSI National Radio Science Meeting*, vol. 3, pp. 1820–1823 vol.3, 1994.

[12] M. E. Bialkowski and K. H. Sayidmarie, "Investigations into phase characteristics of a single-layer reflectarray employing patch or ring elements of variable size," *IEEE Transactions on Antennas and Propagation*, vol. 56, no. 11, pp. 3366–3372, 2008.

[13] J. Huang and J. A. Encinar, *Reflectarray antennas*. John Wiley & Sons, 2007.

[14] J. Huang and R. Pogorzelski, "A ka-band microstrip reflectarray with elements having variable rotation angles," *IEEE Transactions on Antennas and Propagation*, vol. 46, no. 5, pp. 650–656, 1998.

[15] H. R. Phelan, "Spiraphase reflectarray for multitarget radar," *Microwave Journal*, vol. 20, p. 67, July 1977.

[16] L. Boccia, F. Venneri, G. Amendola, and G. Di Massa, "Application of varactor diodes for reflectarray phase control," in *IEEE Antennas and Propagation Society International Symposium (IEEE Cat. No.02CH37313)*, vol. 3, pp. 132–, 2002.

[17] S. Hum, M. Okoniewski, and R. Davies, "Realizing an electronically tunable reflectarray using varactor diode-tuned elements," *IEEE Microwave and Wireless Components Letters*, vol. 15, no. 6, pp. 422–424, 2005.

[18] O. G. Vendik and M. Parnes, "A phase shifter with one tunable component for a reflectarray antenna," *IEEE Antennas and Propagation Magazine*, vol. 50, no. 4, pp. 53–65, 2008.

[19] L. Boccia, G. Amendola, and G. D. Massa, "Performance improvement for a varactor-loaded reflectarray element," *IEEE Transactions on Antennas and Propagation*, vol. 58, no. 2, pp. 585–589, 2010.

[20] S. V. Hum, G. McFeetors, and M. Okoniewski, "Integrated mems reflectarray elements," in *2006 First European Conference on Antennas and Propagation*, pp. 1–6, 2006.

[21] J. Perruisseau-Carrier and A. K. Skrivervik, "Monolithic mems-based reflectarray cell digitally reconfigurable over a 360 ° phase range," *IEEE Antennas and Wireless Propagation Letters*, vol. 7, pp. 138–141, 2008.

[22] H. Legay, Y. Cailloce, O. Vendier, G. Caille, J. Perruisseau-Carrier, M. Lathi, J. P. Polizzi, U. Oestermann, P. Pons, and N. Raveu, "Satellite antennas based on mems tunable reflectarrays," in *The Second European Conference on Antennas and Propagation, EuCAP 2007*, pp. 1–6, 2007.

[23] H. Rajagopalan, Y. Rahmat-Samii, and W. A. Imbriale, "Rf mems actuated reconfigurable reflectarray patch-slot element," *IEEE Transactions on Antennas and Propagation*, vol. 56, no. 12, pp. 3689–3699, 2008.

[24] E. Perret, H. Aubert, and H. Legay, "Scale-changing technique for the electromagnetic modeling of mems-controlled planar phase shifters," *IEEE Transactions on Microwave Theory and Techniques*, vol. 54, no. 9, pp. 3594–3601, 2006.

[25] H. Aubert, N. Raveu, E. Perret, and H. Legay, "Multi-scale approach for the electromagnetic modelling of mems-controlled reflectarrays," in *2006 First European Conference on Antennas and Propagation*, pp. 1–8, 2006.

[26] G. Perez-Palomino, P. Baine, R. Dickie, M. Bain, J. A. Encinar, R. Cahill, M. Barba, and G. Toso, "Design and experimental validation of liquid crystal-based reconfigurable reflectarray elements with improved bandwidth in f-band," *IEEE Transactions on Antennas and Propagation*, vol. 61, no. 4, pp. 1704–1713, 2013.

[27] A. Moessinger, R. Marin, S. Mueller, J. Freese, and R. Jakoby, "Electronically reconfigurable reflectarrays with nematic liquid crystals," *Electronics Letters*, vol. 42, no. 16, pp. 899–900, 2006.

[28] W. Hu, R. Cahill, J. A. Encinar, R. Dickie, H. Gamble, V. Fusco, and N. Grant, "Design and measurement of reconfigurable millimeter wave reflectarray cells with nematic liquid crystal," *IEEE Transactions on Antennas and Propagation*, vol. 56, no. 10, pp. 3112–3117, 2008.

[29] S. Foo, "Liquid-crystal-tunable metasurface antennas," in *2017 11th European Conference on Antennas and Propagation (EUCAP)*, pp. 3026–3030, 2017.

[30] R. Romanofsky, J. Bernhard, F. van Keuls, F. Miranda, G. Washington, and C. Canedy, "K-band phased array antennas based on ba/sub 0.60/sr/sub 0.40/tio/sub

3/ thin-film phase shifters," *IEEE Transactions on Microwave Theory and Techniques*, vol. 48, no. 12, pp. 2504–2510, 2000.

[31] M. Sazegar, A. Giere, Y. Zheng, H. Maune, A. Moessinger, and R. Jakoby, "Reconfigurable unit cell for reflectarray antenna based on barium-strontium-titanate thick-film ceramic," in *2009 European Microwave Conference (EuMC)*, pp. 598–601, 2009.

[32] F. A. Tahir, H. Aubert, and E. Girard, "Equivalent electrical circuit for designing mems-controlled reflectarray phase shifters," *Progress In Electromagnetics Research*, vol. 100, pp. 1–12, 2010.

[33] M. Inam and M. Y. Ismail, "Integration of pin diodes with slot embedded patch elements for active reflectarray antenna design," in *2012 International Symposium on Telecommunication Technologies*, pp. 151–155, 2012.

[34] S. V. Hum, M. Okoniewski, and R. J. Davies, "Modeling and design of electronically tunable reflectarrays," *IEEE Transactions on Antennas and Propagation*, vol. 55, no. 8, pp. 2200–2210, 2007.

[35] L. Boccia, F. Venneri, G. Amendola, and G. Di Massa, "Experimental investigation of a varactor loaded reflectarray antenna," in *2002 IEEE MTT-S International Microwave Symposium Digest (Cat. No.02CH37278)*, vol. 1, pp. 69–73 vol.1, 2002.

[36] X. Yang, S. Xu, F. Yang, M. Li, Y. Hou, S. Jiang, and L. Liu, "A broadband high-efficiency reconfigurable reflectarray antenna using mechanically rotational elements," *IEEE Transactions on Antennas and Propagation*, vol. 65, no. 8, pp. 3959–3966, 2017.

[37] V. Fusco, "Mechanical beam scanning reflectarray," *IEEE Transactions on Antennas and Propagation*, vol. 53, no. 11, pp. 3842–3844, 2005.

[38] R. H. Phillion and M. Okoniewski, "Improving the phase resolution of a micromotor-actuated phased reflectarray," in *2008 1st Microsystems and Nanoelectronics Research Conference*, pp. 169–172, 2008.

[39] C.-W. Baek, S. Song, J.-H. Park, S. Lee, J.-M. Kim, W. Choi, C. Cheon, Y.-K. Kim, and Y. Kwon, "A v-band micromachined 2-d beam-steering antenna driven by magnetic force with polymer-based hinges," *IEEE Transactions on Microwave Theory and Techniques*, vol. 51, no. 1, pp. 325–331, 2003.

[40] M. I. Abbasi, M. H. Dahri, M. H. Jamaluddin, N. Seman, M. R. Kamarudin, and N. H. Sulaiman, "Millimeter wave beam steering reflectarray antenna based on mechanical rotation of array," *IEEE Access*, vol. 7, pp. 145685–145691, 2019.

[41] A. Robinson and M. Bialkowski, "An x-band active microstrip reflectarray," in *Proceedings of 1997 Asia-Pacific Microwave Conference*, vol. 3, pp. 925–928 vol.3, 1997.

[42] A. W. Robinson, M. E. Bialkowski, and H. J. Song, "A 137-element active reflect array with dual-feed microstrip patch elements," *Microwave and Optical Technology Letters*, vol. 26, no. 3, pp. 147–151, 2000.

[43] M. Bialkowski and H. Song, "Investigations into a power-combining structure using a reflectarray of dual-feed aperture-coupled microstrip patch antennas," *IEEE Transactions on Antennas and Propagation*, vol. 50, no. 6, pp. 841–849, 2002.

[44] R. Hodges and M. Zawadzki, "Design of a large dual polarized ku band reflectarray for space borne radar altimeter," in *IEEE Antennas and Propagation Society Symposium, 2004.*, vol. 4, pp. 4356–4359 Vol.4, 2004.

[45] B. Khayatian and Y. Rahmat-Samii, "A novel antenna concept for future solar sails: application of fresnel antennas," *IEEE Antennas and Propagation Magazine*, vol. 46, no. 2, pp. 50–63, 2004.

[46] J. Pendry, "Metamaterials and the control of electromagnetic fields," in *Conference on Coherence and Quantum Optics*, p. CMB2, Optical Society of America, 2007.

[47] C. Caloz and T. Itoh, "Transmission line approach of left-handed (lh) materials and microstrip implementation of an artificial lh transmission line," *IEEE Transactions on Antennas and Propagation*, vol. 52, no. 5, pp. 1159–1166, 2004.

[48] I. V. Lindell, S. A. Tretyakov, K. I. Nikoskinen, and S. Ilvonen, "Bw media—media with negative parameters, capable of supporting backward waves," *Microwave and Optical Technology Letters*, vol. 31, no. 2, pp. 129–133, 2001.

[49] R. W. Ziolkowski and E. Heyman, "Wave propagation in media having negative permittivity and permeability," *Phys. Rev. E*, vol. 64, p. 056625, Oct 2001.

[50] D. S. Weile, "Electromagnetic metamaterials: Physics and engineering explorations (engheta, n. and ziolkowski, rw; 2006)[book review]," *IEEE Antennas and Propagation Magazine*, vol. 49, no. 4, pp. 137–139, 2007.

[51] S. S. Bukhari, J. Y. Vardaxoglou, and W. Whittow, "A metasurfaces review: Definitions and applications," *Applied Sciences*, vol. 9, no. 13, p. 2727, 2019.

[52] E. F. Kuester, M. A. Mohamed, M. Piket-May, and C. L. Holloway, "Averaged transition conditions for electromagnetic fields at a metafilm," *IEEE Transactions on Antennas and Propagation*, vol. 51, no. 10, pp. 2641–2651, 2003.

[53] D. R. Smith, J. B. Pendry, and M. C. Wiltshire, "Metamaterials and negative refractive index," *Science*, vol. 305, no. 5685, pp. 788–792, 2004.

[54] A. V. Kildishev, A. Boltasseva, and V. M. Shalaev, "Planar photonics with metasurfaces," *Science*, vol. 339, no. 6125, p. 1232009, 2013.

[55] B. A. Munk, *Frequency selective surfaces: theory and design*. John Wiley & Sons, 2005.

[56] A. K. Rashid, B. Li, and Z. Shen, "An overview of three-dimensional frequency-selective structures," *IEEE Antennas and Propagation Magazine*, vol. 56, no. 3, pp. 43–67, 2014.

[57] N. Yu and F. Capasso, "Flat optics with designer metasurfaces," *Nature materials*, vol. 13, no. 2, pp. 139–150, 2014.

[58] S. B. Glybovski, S. A. Tretyakov, P. A. Belov, Y. S. Kivshar, and C. R. Simovski, "Metasurfaces: From microwaves to visible," *Physics Reports*, vol. 634, pp. 1–72, 2016. Metasurfaces: From microwaves to visible.

[59] Z. Luo, L. Zhao, C. Xue, and D. Sievenpiper, "An electrically tunable absorbing metasurface for surface waves and plane waves," in *2016 Asia-Pacific Microwave Conference (APMC)*, pp. 1–4, 2016.

[60] K. Achouri and C. Caloz, "Design, concepts, and applications of electromagnetic metasurfaces," *Nanophotonics*, vol. 7, no. 6, pp. 1095–1116, 2018.

[61] L. Zheng and Y. Zhao, "Generalized snell's law and its verification by metasurface," in *Innovative Mobile and Internet Services in Ubiquitous Computing* (L. Barolli, A. Poniszewska-Maranda, and H. Park, eds.), (Cham), pp. 364–372, Springer International Publishing, 2021.

[62] J. Ginn, B. Lail, J. Alda, and G. Boreman, "Planar infrared binary phase reflectarray," *Optics letters*, vol. 33, no. 8, pp. 779–781, 2008.

[63] M. Farmahini-Farahani and H. Mosallaei, "Birefringent reflectarray metasurface for beam engineering in infrared," *Optics letters*, vol. 38, no. 4, pp. 462–464, 2013.

[64] T. Niu, W. Withayachumnankul, A. Upadhyay, P. Gutruf, D. Abbott, M. Bhaskaran, S. Sriram, and C. Fumeaux, "Terahertz reflectarray as a polarizing beam splitter," *Opt. Express*, vol. 22, pp. 16148–16160, Jun 2014.

[65] D. Micheli, R. Pastore, A. Vricella, and M. Marchetti, "Matter's electromagnetic signature reproduction by graded-dielectric multilayer assembly," *IEEE Transactions on Microwave Theory and Techniques*, vol. 65, no. 8, pp. 2801–2809, 2017.

[66] C.-N. Chiu and K.-P. Chang, "A novel miniaturized-element frequency selective surface having a stable resonance," *IEEE Antennas and Wireless Propagation Letters*, vol. 8, pp. 1175–1177, 2009.

[67] K. Sarabandi and N. Behdad, "A frequency selective surface with miniaturized elements," *IEEE Transactions on Antennas and Propagation*, vol. 55, no. 5, pp. 1239–1245, 2007.

[68] X. Chen, J. Gao, C. Fang, N. Xu, Y. Wang, and Y. Tang, "Deformable frequency selective surface structure with tuning capability through thermoregulating," *Opt. Express*, vol. 23, pp. 16329–16338, Jun 2015.

[69] B. Sanz-Izquierdo, E. A. Parker, J.-B. Robertson, and J. C. Batchelor, "Singly and dual polarized convoluted frequency selective structures," *IEEE Transactions on Antennas and Propagation*, vol. 58, no. 3, pp. 690–696, 2010.

[70] F. Falcone, T. Lopetegi, M. A. G. Laso, J. D. Baena, J. Bonache, M. Beruete, R. Marqués, F. Martín, and M. Sorolla, "Babinet principle applied to the design of metasurfaces and metamaterials," *Phys. Rev. Lett.*, vol. 93, p. 197401, Nov 2004.

[71] Y. Ra'di, V. S. Asadchy, and S. A. Tretyakov, "One-way transparent sheets," *Phys. Rev. B*, vol. 89, p. 075109, Feb 2014.

[72] X.-D. Hu, X.-L. Zhou, L.-S. Wu, L. Zhou, and W.-Y. Yin, "A miniaturized dual-band frequency selective surface (fss) with closed loop and its complementary pattern," *IEEE Antennas and Wireless Propagation Letters*, vol. 8, pp. 1374–1377, 2009.

[73] R.-R. Xu, Z.-Y. Zong, and W. Wu, "Low-frequency miniaturized dual-band frequency selective surfaces with close band spacing," *Microwave and Optical Technology Letters*, vol. 51, pp. 1238–1240, Sep 2008.

[74] A. V. Bessarab, N. V. Zhidkov, S. B. Kormer, D. Pavlov, and A. I. Funtikov, "Measurement of the reflectivity of metal mirrors acted on by laser radiation," *Soviet Journal of Quantum Electronics*, vol. 8, no. 2, p. 188, 1978.

[75] D. Pozar, "Input impedance and mutual coupling of rectangular microstrip antennas," *IEEE Transactions on Antennas and Propagation*, vol. 30, no. 6, pp. 1191–1196, 1982.

[76] D. Sievenpiper, L. Zhang, R. F. J. Broas, N. G. Alexopolous, and E. Yablonovitch, "High-impedance electromagnetic surfaces with a forbidden frequency band," *IEEE Transactions on Microwave Theory and Techniques*, vol. 47, no. 11, pp. 2059–2074, 1999.

[77] S. Maci and P.-S. Kildal, "Hard and soft surfaces realized by fss printed on a grounded dielectric slab," in *IEEE Antennas and Propagation Society Symposium, 2004.*, vol. 1, pp. 285–288 Vol.1, 2004.

[78] L. Li, J. Wang, J. Wang, H. Ma, H. Du, J. Zhang, S. Qu, and Z. Xu, "Reconfigurable all-dielectric metamaterial frequency selective surface based on high-permittivity ceramics," *Scientific reports*, vol. 6, no. 1, pp. 1–8, 2016.

[79] T. Debogović, J. Bartolić, and J. Perruisseau-Carrier, "Dual-polarized partially reflective surface antenna with mems-based beamwidth reconfiguration," *IEEE Transactions on Antennas and Propagation*, vol. 62, no. 1, pp. 228–236, 2014.

[80] F. Bayatpur and K. Sarabandi, "Design and analysis of a tunable miniaturized-element frequency-selective surface without bias network," *IEEE Transactions on Antennas and Propagation*, vol. 58, no. 4, pp. 1214–1219, 2010.

[81] H.-T. Chen, W. J. Padilla, J. M. Zide, A. C. Gossard, A. J. Taylor, and R. D. Averitt, "Active terahertz metamaterial devices," *Nature*, vol. 444, no. 7119, pp. 597–600, 2006.

[82] D. Sievenpiper, J. H. Schaffner, H. J. Song, R. Y. Loo, and G. Tangonan, "Two-dimensional beam steering using an electrically tunable impedance surface," *IEEE Transactions on Microwave Theory and Techniques*, vol. 51, no. 10, pp. 2713–2722, 2003.

[83] "Rf/microwave capacitors - https://datasheets.kyocera-avx.com/600s.pdf."

APPENDICES

Appendix A

MATLAB codes for phase distribution

```
clear;
close all;
nx=40;%numbers of array at x direction
ny=40;%numbers of array at y direction
p=0.026;%element length
f=3.5*10^9;%working frequency
k=2*pi*f/(3*10^8);%wavelength constant
fx=-0.01;%x of feed
fy=0;%y of feed
fz=1;%z of feed
theta=deg2rad(0);%steering angle theta
phi=deg2rad(0);%steering angle phi
C=zeros(nx,ny);%phase of each element
x = linspace(1,nx,nx);%X axis No.
y = linspace(1,ny,ny);%Y axis No.
dx = linspace(-(nx-1)*p/2,(nx-1)*p/2,nx);%x distance to center
dy = linspace(-(ny-1)*p/2,(ny-1)*p/2,ny);%y distance to center
for i=1:ny
    for j=1:nx
        phi_sp=-k*sqrt((dx(j)-fx)^2+(dy(i)-fy)^2+fz^2)+k*sqrt((0-fx)
   ^2+(0-fy)^2+fz^2);
        phi_pp=-k*(dx(j)*sin(theta)*cos(phi)+dy(i)*sin(theta)*sin(phi));
        C(i,j)=rad2deg(wrapTo2Pi(phi_pp-phi_sp));
    end
end
plot(1:nx);
axis([1 40 1 40])
```

```
hold on;
image(C,'CDataMapping','scaled')
xlabel('X axis No.');
ylabel('Y axis No.');
colorbar;
```

Listing A.1: Matlab codes of phase distribution